

Methoxy-naphthyl-Linked *N*-Benzyl Pyridinium Styryls as Dual Cholinesterase Inhibitors: Design, Synthesis, Biological Evaluation, and Structure–Activity Relationship

Mohd Abdullaha, Razia Banoo, Vijay K. Nuthakki, Mohit Sharma, Sukhleen Kaur, Shikha Thakur, Ajay Kumar, Hemant R. Jadhav, and Sandip B. Bharate*



Cite This: *ACS Omega* 2023, 8, 17591–17608



Read Online

ACCESS |



Metrics & More

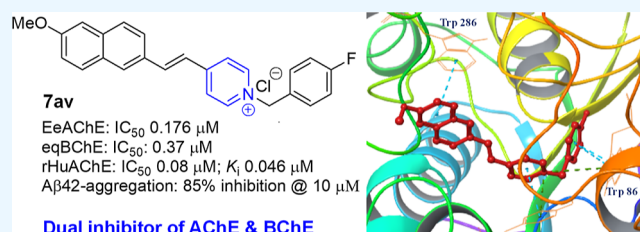


Article Recommendations



Supporting Information

ABSTRACT: The multifaceted nature of Alzheimer's disease (AD) indicates the need for multitargeted agents as potential therapeutics. Both cholinesterases (ChEs), acetylcholinesterase (AChE) and butyrylcholinesterase (BChE), play a vital role in disease progression. Thus, inhibiting both ChEs is more beneficial than only one for effectively managing AD. The present study provides a detailed lead optimization of the *e*-pharmacophore-generated pyridinium styryl scaffold to discover a dual ChE inhibitor. A structure–activity relationship analysis indicated the importance of three structural fragments, methoxy-naphthyl, vinyl-pyridinium, and substituted-benzyl, in a dual ChE inhibitor pharmacophore. The optimized 6-methoxy-naphthyl derivative, **7av** (SB-1436), inhibits EeAChE and eqBChE with IC₅₀ values of 176 and 370 nM, respectively. The kinetic study has shown that **7av** inhibits AChE and BChE in a non-competitive manner with *k_i* values of 46 and 115 nM, respectively. The docking and molecular dynamics simulation demonstrated that **7av** binds with the catalytic and peripheral anionic sites of AChE and BChE. Compound **7av** also significantly stops the self-aggregation of Aβ. The data presented herein indicate the potential of **7av** for further investigation in preclinical models of AD.



1. INTRODUCTION

Alzheimer's disease (AD) is a neurodegenerative disorder characterized by memory loss and cholinergic deficit.^{1–3} The World Health Organization has forecasted that AD will dominate AIDS and cancer over the next century.⁴ The primary hallmarks of AD are central cholinergic depletion and Aβ plaque formation.^{5,6} Several neurochemical factors are associated with AD initiation and progression.⁷ To date, the exact cause of AD is not well-ascertained; however, various proposed hypotheses rest on experimental pathophysiological factors.^{8–10} The cholinergic theory is the most widely investigated, postulating that acetylcholine (ACh) deficiency causes AD.^{2,11,12} The ACh deficiency occurs either due to decreased production or increased enzymatic degradation by acetylcholinesterase (AChE).¹³ Besides, AChE also plays a vital role in forming Aβ plaques.^{14–16} Consequently, the inhibition of AChE is considered an important therapeutic target in the drug discovery program for AD.^{17,18} The inhibition of AChE helps increase ACh concentrations in the brain and reduces the AChE-assisted deposition of toxic Aβ plaques. However, in the advanced stage of AD, the activity of AChE is surrogated by the BChE (*pseudo*-ChE). As a result, the inhibition of both AChE and BChE concurrently is equally essential.^{19–23}

Four FDA-approved AChE inhibitors are tacrine, donepezil, rivastigmine, and galantamine.²⁴ However, tacrine has been discontinued because of its high hepatotoxicity,²⁵ while other

three AChE inhibitors offer merely a symptomatic relief.²⁶ Enormous efforts have been made to discover selective AChE inhibitors in the past few years;^{27–40} however, there are not many scaffolds with dual AChE/BChE inhibition. Rivastigmine is the known dual ChE inhibitor but has high micromolar inhibitory activity. Continuing our previous efforts, we conducted the medicinal chemistry of the pyridinium styryl scaffold, which was identified previously via the *e*-pharmacophore approach.²⁰ Thus, herein, we report the synthesis and structure–activity relationship studies of the benzylpyridinium styryl series for dual ChE inhibition.

2. RESULTS AND DISCUSSION

2.1. Design. We recently optimized the *e*-pharmacophore-generated *N*-benzyl pyridinium benzamide scaffold to find new dual ChE inhibitors that provided a methoxy-naphthyl derivative SB-1389 as a dual ChE inhibitor.²⁰ Continuing this study, we synthesized and optimized another *e*-

Received: December 24, 2022

Accepted: April 25, 2023

Published: May 9, 2023



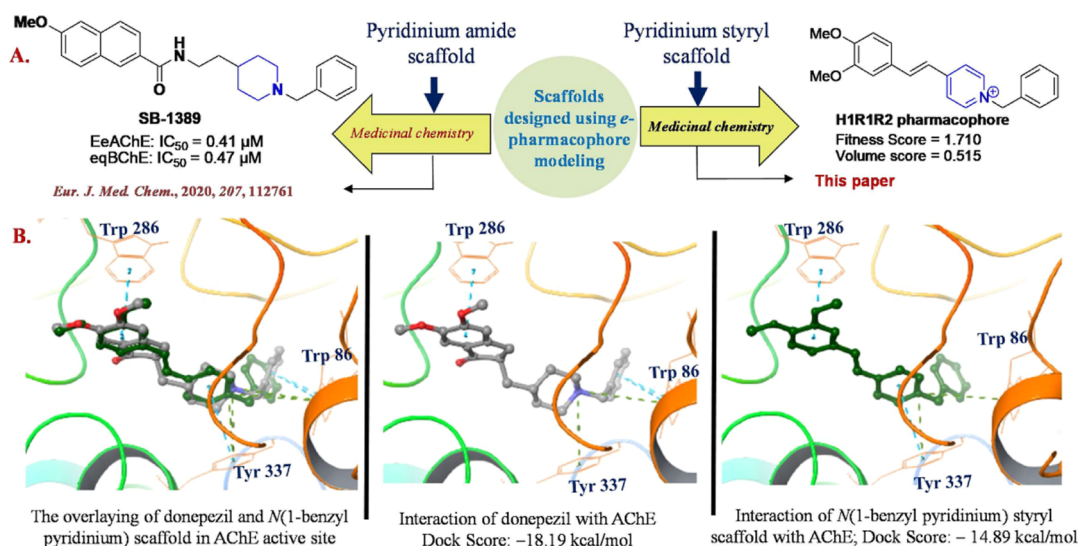
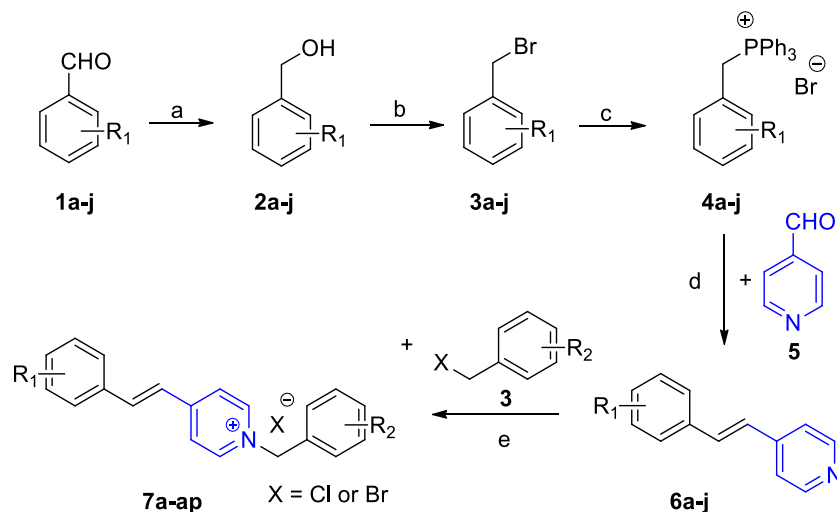


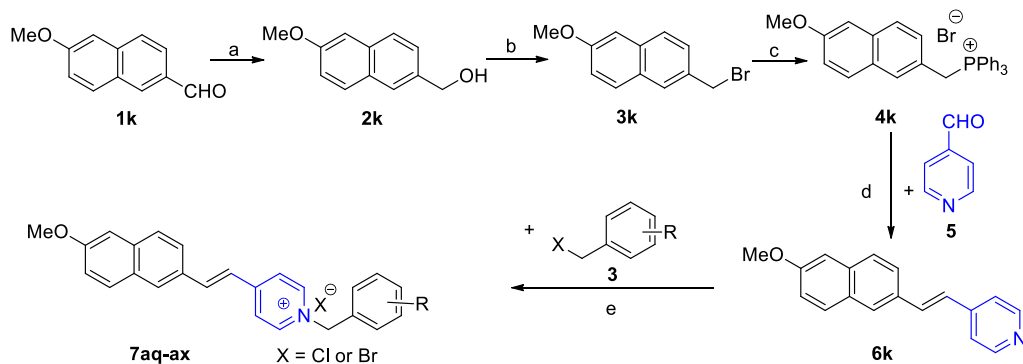
Figure 1. (A) Design of potential scaffolds via *e*-pharmacophore modeling and their medicinal chemistry to identify a potential dual inhibitor of AChE and BChE; (B) interaction of the donepezil and *N*-benzyl pyridinium styryl scaffold with the active site of AChE. The donepezil and pyridinium styryl are shown in gray and green colors, respectively.

Scheme 1. Synthesis of Phenyl-Containing *N*-Benzyl Pyridinium Styryls, 7a–7ap^a

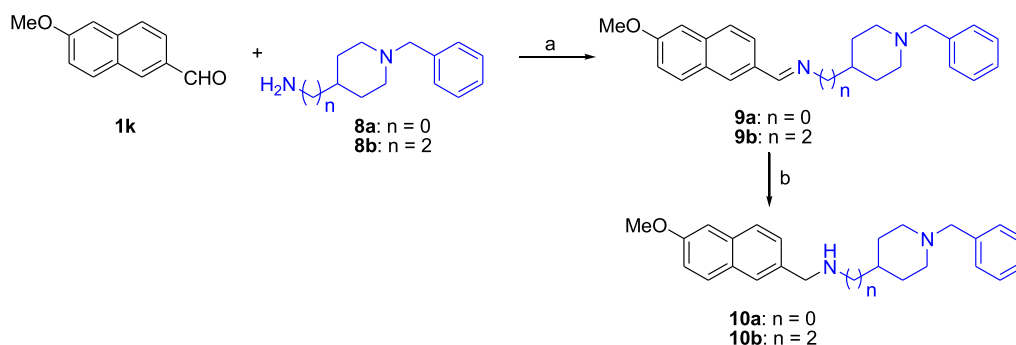


^aReagents and conditions: (a) NaBH_4 (1.5 equiv), MeOH, 0 °C, 30 min, >97% yield; (b) NBS, PPh_3 , DCM, 60 °C, 30 min, 90%; (c) PPh_3 , 80 °C, THF, 1 h, >97% yield; (d) *t*-BuOK, Dry THF, 80 °C, 1 h, >80% yield; and (e) ACN, 80 °C, 3 h, 85–95% yield.

Scheme 2. Synthesis of Naphthyl-Containing *N*-Benzyl Pyridinium Styryls, 7aq–ax^a



^aReagents and conditions: (a) NaBH_4 (1.5 equiv), MeOH, 0 °C, 30 min, 97% yield; (b) NBS, PPh_3 , DCM, 60 °C, 30 min, 97% yield; (c) PPh_3 , 80 °C, THF, 1 h, 92% yield; (d) *t*-BuOK, Dry THF, 80 °C, 1 h, 80% yield; and (e) ACN, 80 °C, 3 h, 85–95% yield.

Scheme 3. Synthesis of Piperidinyl Analogues, 10a–b^a

^aReagents and conditions: (a) glacial acetic acid (2–3 drops), ethanol, rt, 6–7 h, 80% and (b) NaBH₄, methanol, rt, 3–4 h, 56–68%.

Table 1. Inhibition of ChEs by *N*-Benzyl Pyridinium Styryls Bearing Electron-Donating Groups on the Phenyl Moiety (Ring A)^a

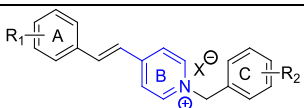
Entry	R ₁	R ₂	X	Percentage inhibition / IC ₅₀			
				AChE		BChE	
				% Inhibition ± SD @ 1 μM	IC ₅₀ ± SD (μM)	% Inhibition ± SD @ 1 μM	IC ₅₀ ± SD (μM)
7a	3,5-di-OMe	H	Br	93.65 ± 0.90	0.08 ± 0.010	20.78 ± 1.10	nd
7b	3,5-di-OMe	2-Me	Br	83.07 ± 2.45	0.32 ± 0.015	14.51 ± 1.33	nd
7c	3,5-di-OMe	2-Cl	Cl	93.07 ± 0.54	0.13 ± 0.014	34.16 ± 3.55	nd
7d	3,5-di-OMe	3-Cl	Cl	79.18 ± 2.37	0.39 ± 0.021	15.99 ± 1.75	nd
7e	3,5-di-OMe	4-Cl	Cl	24.66 ± 1.54	nd	13.36 ± 1.73	nd
7f	3,5-di-OMe	2-F	Br	93.71 ± 0.45	0.20 ± 0.002	16.11 ± 1.57	nd
7g	3,5-di-OMe	4-F	Cl	94.10 ± 2.79	0.15 ± 0.020	19.55 ± 2.24	nd
7h	3,5-di-OMe	2-NO ₂	Br	56.68 ± 1.77	0.37 ± 0.017	6.74 ± 0.97	nd
7i	3,5-di-OMe	4-NO ₂	Br	15.36 ± 2.62	nd	7.33 ± 1.32	nd
7j	3,4-di-OMe	H	Br	73.86 ± 1.50	0.46 ± 0.009	9.35 ± 2.05	nd
7k	3,4-di-OMe	2-Me	Br	59.78 ± 4.25	0.626 ± 0.017	25.54 ± 1.97	nd
7l	3,4-di-OMe	2-Cl	Cl	13.36 ± 1.64	nd	25.12 ± 2.25	nd
7m	3,4-di-OMe	4-F	Cl	69.25 ± 2.88	0.55 ± 0.045	4.00 ± 2.00	nd
7n	3,4-di-OMe	4-NO ₂	Br	16.30 ± 2.15	nd	1.72 ± 0.45	nd
7o	3,4,5-tri-OMe	2-Me	Br	50.48 ± 2.48	0.66 ± 0.038	27.77 ± 2.18	nd
7p	3,4,5-tri-OMe	2-Cl	Cl	68.62 ± 4.22	0.46 ± 0.024	86.61 ± 1.38	0.53 ± 0.022
7q	3,4,5-tri-OMe	4-F	Cl	64.78 ± 2.91	0.68 ± 0.041	74.69 ± 4.49	0.36 ± 0.004
7r	3,4,5-tri-OMe	2-NO ₂	Br	1.13 ± 1.59	nd	1.13 ± 1.59	nd
7s	3,4,5-tri-OMe	4-NO ₂	Br	1.72 ± 0.45	nd	14.51 ± 1.33	nd
7t	4-OMe	H	Br	52.40 ± 4.15	0.53 ± 0.040	13.12 ± 2.01	nd
7u	4-OMe	2-F	Cl	73.91 ± 2.53	0.36 ± 0.002	14.08 ± 1.06	nd
7v	4-OMe	2-NO ₂	Br	36.38 ± 4.72	nd	5.76 ± 1.28	nd
7w	4-OEt	H	Br	70.64 ± 5.90	0.52 ± 0.022	44.73 ± 3.31	nd
7x	4-OEt	2-Me	Br	45.80 ± 4.44	nd	33.54 ± 1.56	nd
7y	4-OEt	2-Cl	Cl	71.00 ± 1.72	0.58 ± 0.027	0.65 ± 0.018	nd
7z	4-OEt	4-Cl	Cl	22.36 ± 7.69	nd	22.36 ± 7.69 ^a	nd
7aa	4-OEt	2-F	Br	72.47 ± 2.26	0.395 ± 0.013	40.20 ± 0.65	nd
7ab	4-OEt	2-NO ₂	Br	48.08 ± 0.004	nd	15.40 ± 1.72	nd
Donepezil				98.36 ± 1.52	0.045 ± 0.03	24.71 ± 2.29	5.25 ± 0.23

^and = not determined.

pharmacophore-generated *N*-benzyl pyridinium styryl scaffold. The docking study demonstrates the interaction of pyridinium styryl with the peripheral anionic site (PAS) and catalytic anionic sites (CASs) of AChE in the same way as donepezil. The phenyl moiety shows π - π stacking interactions with the PAS residue Trp 286, whereas the quaternary nitrogen builds π -cation contacts with CAS residues Trp 86 and Tyr 337. Furthermore, the benzyl moiety attains a position to stack with Trp 86 (Figure 1).

2.2. Synthesis of *N*-Benzyl Pyridinium Styryl Derivatives. The synthesis of pyridinium styryls 6a–k started with aryl aldehydes 1a–k, which were reduced to the corresponding benzyl alcohols 2a–k using NaBH₄ in methanol at 0 °C. Benzyl alcohols 2a–k on treatment with triphenylphosphine (PPh₃) and *N*-bromosuccinamide (NBS) afforded the corresponding benzyl bromides, 3a–k. This was followed by synthesizing Wittig's salt, 4a–k, by treating benzyl bromides 3a–k with PPh₃ in THF for 3 h. Different pyridine styryls, 6a–k, were synthesized by treating Wittig's salt, 4a–k, with

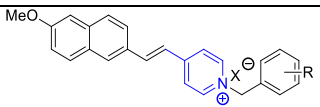
Table 2. Inhibition of ChEs by *N*(1-Benzyl Pyridinium) Styryls Bearing Electron-Withdrawing Groups on the Phenyl Moiety (Ring A)^a



Entry	R ₁	R ₂	X	Percentage inhibition / IC ₅₀			
				AChE		BChE	
				% Inhibition ± SD @ 1 μM	IC ₅₀ ± SD (μM)	% Inhibition ± SD @ 1 μM	IC ₅₀ ± SD (μM)
7ac	4-Br	H	Br	39.82 ± 2.34	nd	21.44 ± 0.54	nd
7ad	4-Br	2-Cl	Cl	69.88 ± 3.80	0.47 ± 14.8	37.92 ± 2.16	nd
7ae	4-Br	2-F	Br	75.47 ± 3.16	0.36 ± 0.025	19.64 ± 0.97	nd
7af	4-Br	4-F	Cl	25.90 ± 4.05	nd	30.60 ± 0.56	nd
7ag	4-Cl	H	Br	45.55 ± 1.22	nd	28.82 ± 1.41	nd
7ah	4-Cl	2-Me	Br	17.45 ± 1.86	nd	20.49 ± 1.30	nd
7ai	4-Cl	2-Cl	Cl	65.04 ± 2.13	0.57 ± 0.026	33.75 ± 2.41	nd
7aj	4-Cl	4-Cl	Cl	9.32 ± 2.97	nd	37.97 ± 2.91	nd
7ak	4-Cl	4-F	Cl	32.92 ± 3.35	nd	31.75 ± 2.34	nd
7al	4-Cl	4-NO ₂	Br	27.89 ± 2.46	nd	17.86 ± 1.74	nd
7am	3-Cl	H	Br	50.70 ± 2.67	0.47 ± 0.022	18.95 ± 2.28	nd
7an	4-NO ₂	H	Br	64.66 ± 0.68	0.57 ± 0.016	14.87 ± 1.73	nd
7ao	4-NO ₂	2-Me	Br	52.18 ± 1.78	0.63 ± 0.024	11.03 ± 1.39	nd
7ap	4-NO ₂	4-F	Cl	55.56 ± 3.04	0.56 ± 0.032	17.90 ± 1.63	nd
Donepezil				98.36 ± 1.52	0.045 ± 0.03	24.71 ± 2.29	5.25 ± 0.23

^and = not determined.

Table 3. Inhibition of ChEs by Naphthalene-Linked *N*(1-Benzyl Pyridinium) Styryls, 7aq–7ax^a



Entry	R	X	Percentage inhibition / IC ₅₀			
			AChE		BChE	
			% Inhibition ± SD @ 1 μM	IC ₅₀ ± SD (μM)	% Inhibition ± SD @ 1 μM	IC ₅₀ ± SD (μM)
7aq	H	Br	89.68 ± 1.80	0.24 ± 0.013	60.24 ± 0.06	0.76 ± 0.017
7ar	2-Me	Br	89.68 ± 1.80	0.93 ± 0.021	46.32 ± 1.59	nd
7as	2-Cl	Cl	51.24 ± 2.57	0.28 ± 0.020	96.02 ± 0.33	0.19 ± 0.005
7at	4-Cl	Cl	25.26 ± 1.05	nd	25.26 ± 1.05	nd
7au	2-F	Br	90.07 ± 1.63	0.30 ± 0.022	56.71 ± 3.17	0.74 ± 0.005
7av	4-F	Cl	93.21 ± 1.42	0.176 ± 0.007	75.92 ± 3.07	0.37 ± 0.028
7aw	2-NO ₂	Br	21.93 ± 3.15	nd	25.74 ± 2.63	nd
7ax	4-NO ₂	Br	22.48 ± 3.33	nd	13.19 ± 1.76	nd
Donepezil	-	-	98.36 ± 1.52	0.045 ± 0.03	24.71 ± 2.29	5.25 ± 0.23

^and = not determined.

pyridine-4-carboxaldehyde (**5**) under a reflux condition at 80 °C. Finally, the pyridinium styryls **7aq–ax** were prepared by refluxing pyridine styryls **5a–k** and benzyl halides in acetonitrile (ACN) at 80 °C for 3 h (Schemes 1 and 2). Interestingly, the integration of aryl proton signals of unsubstituted and Me- or halogen-substituted benzyl in the ¹H NMR for pyridinium styryls is lower. This could be because of the partial exchange of these protons with deuterium from CD₃OD. In particular, the fluoro-substituted benzyls have shown much-pronounced aryl proton exchange.

For the structure–activity relationship, the central vinyl pyridine region was also replaced with an amino-piperidinyll unit, and three representative analogues, **9a**, **10a**, **10b**, were synthesized, as depicted in Scheme 3.

2.3. In vitro ChE Inhibition. All synthesized compounds were tested in the Ellman assay to inhibit EeAChE and

eqBChE at 1 μM. Compounds showing >50% inhibition of AChE and BChE were considered for IC₅₀ determination. Most compounds exhibited IC₅₀ < 1 μM for AChE, and few have shown IC₅₀ < 1 μM for BChE. During lead optimization studies, phenyl and benzyl rings were substituted with different electron-donating and electron-withdrawing groups, and the phenyl moiety was also replaced with naphthalene. The compounds with R₁ = OMe at the 3rd and 5th positions (i.e., **7a**, **7b**, **7c**, and **7g**) of phenyl display higher inhibition of AChE than compounds carrying R₁ = OMe at the 3rd and 4th positions of phenyl (i.e., **7j**, **7k**, **7l**, and **7m**). Furthermore, increasing the number of methoxy groups to three on the phenyl ring decreases the activity, which is evident by comparing **7b**, **7c**, and **7g** with **7o**, **7p**, and **7q**, respectively (Table 1). Compounds bearing methoxy and ethoxy groups at the 4th position of phenyl also display an excellent anti-AChE

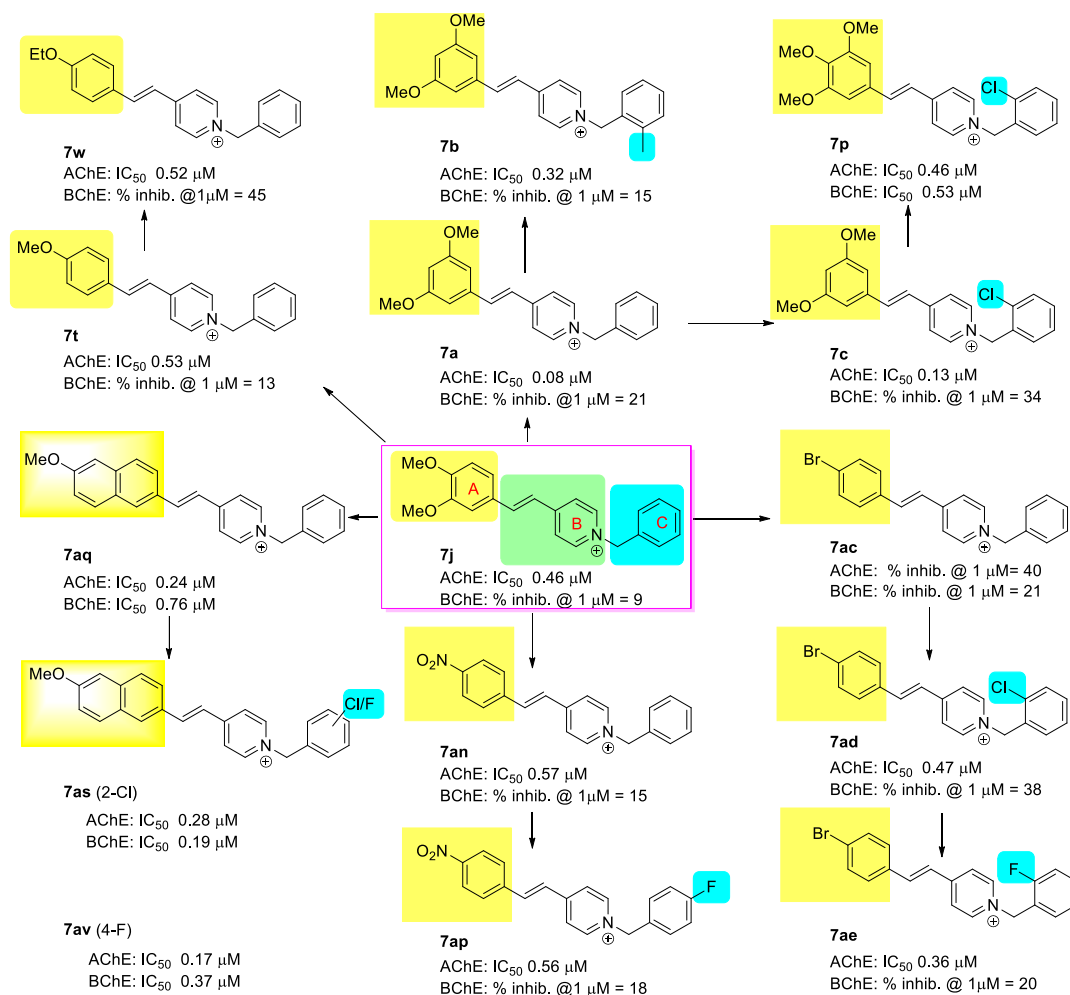


Figure 2. Structure–activity relationship of the *N*(1-benzyl pyridinium) styryl framework against ChEs depicting the effect of A- and C-ring modifications.

profile. The substitution of a powerful electron-withdrawing group $-\text{NO}_2$ on the benzyl group (e.g., **7a** vs **7h** and **7i**) reduces the activity. The number of $-\text{OMe}$ groups on ring A directly impacts BChE inhibition. Trimethoxy-pyridinium styryls (e.g., **7p**) show significantly superior inhibition of BChE compared to the dimethoxy counterpart, **7c** (Table 1).

Furthermore, we prepared compounds bearing phenyl (ring A) substituted with moderate electron-withdrawing groups, $-\text{Cl}$ and $-\text{Br}$. These groups did not significantly increase potency against AChE, and none of the compounds showed $>50\%$ inhibition of BChE at the tested concentration (Table 2).

As observed in Table 1 and based on the literature precedence, the bulkier hydrophobic functionalities at the PAS binding pharmacophore helps to boost BChE inhibition. Thus, we synthesized naphthalene-linked *N*(1-benzyl pyridinium) styryls and substituted the benzyl moiety (ring C) with different EDGs and EWGs. Replacing the phenyl moiety (ring A) with naphthalene ameliorated the inhibitory potential against BChE. This is evident by comparing the activity potential of **7a** and **7aq** (20 vs 60% inhibition of BChE at 1 μM). The Cl moiety at the 2nd position and $-\text{F}$ at the 4th position of benzyl (ring C) play a vital role in attaining dual potency. This series's most potent analogue, **7av**, exhibited dual anti-AChE/BChE activity with IC₅₀ values of 0.176 and

0.37 μM, respectively (Table 3). Compound **7av** also inhibits recombinant human AChE with an IC₅₀ value of 0.08 μM.

2.4. Structure–Activity Relationship. The shift of the methoxy group from 3,4 to 3,5 positions on the phenyl ring (ring A) of *N*(1-benzyl pyridinium) styryl framework considerably increases the efficacy against AChE (**7j** vs **7a**). The substitution of methyl on the benzyl moiety decreases the activity (compound **7b**). In contrast, the $-\text{Cl}$ group (**7c**) at the same position surges the action for both enzymes. Furthermore, the tri-methoxy-substituted *N*(1-benzyl pyridinium) styryl with the chloro at the 2nd position of benzyl considerably enhances anti-BChE potential (compound **7p**). Removing a methoxy group from the third position of **7j** decreases activity against AChE (**7t**). The exchange of methoxy with the ethoxy functionality at the 4th position increases the activity against BChE (**7w**). Furthermore, substituting the phenyl ring with electron-withdrawing groups such as $-\text{NO}_2$ (compound **7an**) decreases the efficacy against AChE and BChE. The substitution of $-\text{Cl}$ at the phenyl (ring A) drastically reduces the therapeutic effectiveness against AChE (**7ag**); however, the activity is re-gained on further substitution of $-\text{Cl}$ on the benzyl (ring C) (**7ai**). Bromo-substitution on phenyl decreases the activity potential against AChE (**7ac**), but further substituting the fluoro (**7ae**) or chloro (**7ad**) group on ring C ameliorates the anti-ChE activity potential. Furthermore, the exchange of phenyl with naphthyl

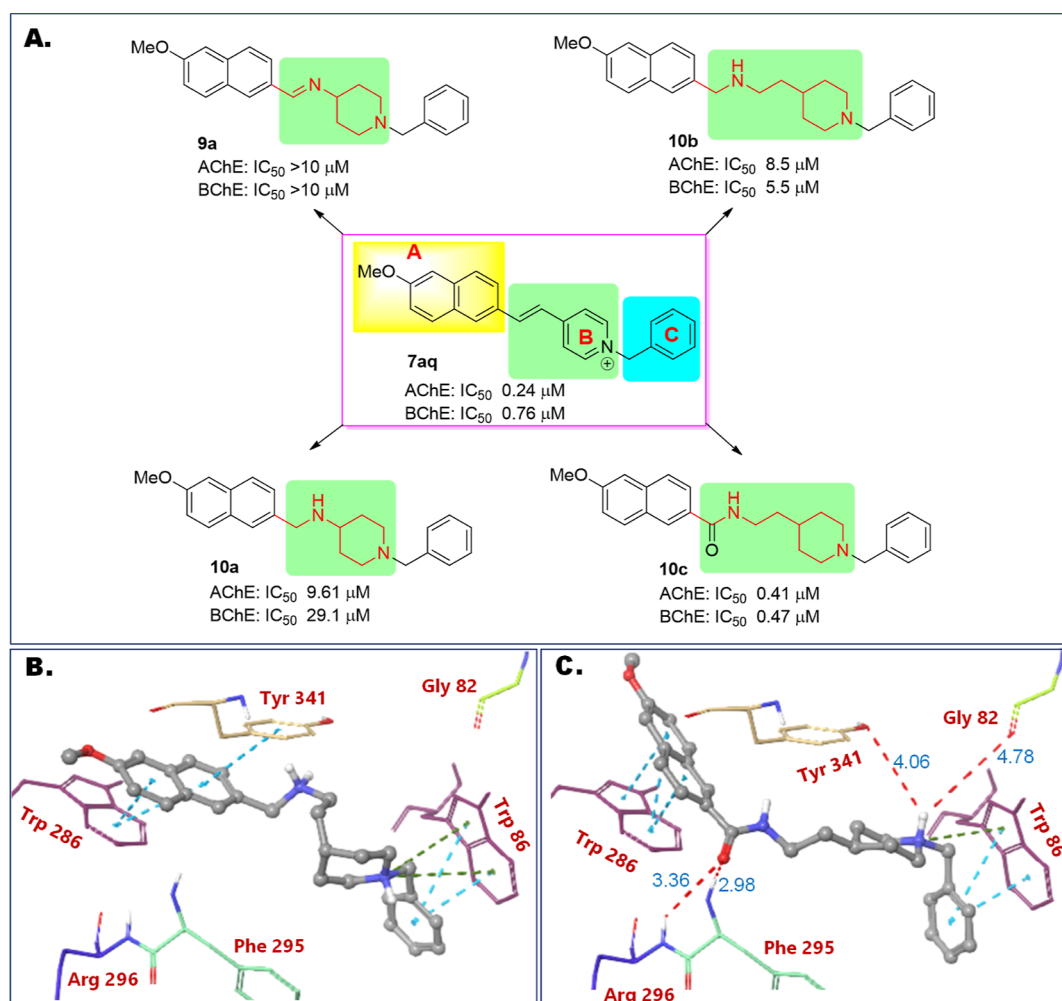


Figure 3. (A) Structure–activity relationship of the *N*(1-benzyl pyridinium) styryl framework against cholinesterases depicting the effect of B-ring modifications and (B,C) differences in the interaction of **10b** (B) and **10c** (C) with AChE. Red dotted lines are H-bond interactions, whereas the blue dotted lines are π – π interactions.

results in a considerable surge in the activity against AChE and BChE. Additionally, the substitution of chloro (**7as**) or fluoro (**7av**) on benzyl of naphthyl *N*(1-benzyl pyridinium) further improves the dual inhibition potency. In a nutshell, the position of –Cl and –F on the benzyl moiety of the *N*(1-benzyl pyridinium) styryl layout is crucial for accomplishing dual AChE/BChE inhibition competence (Figure 2).

A selected set of derivatives were synthesized by replacing the central vinyl-pyridinyl unit with the amino-piperidinyl moiety to understand the structure–activity relationship. The AChE and BChE inhibition data of these series of vinyl-pyridinyl-region modified analogues, **9a**, **10a**, **10b**, are depicted in Figure 3A. Replacing vinyl-pyridinyl with flexible piperidinyl units (e.g., **9a** and **10a**) without varying the linker length yielded compounds with significantly reduced ChE inhibition. The analogue **10b** with the elongated linker is slightly better than **10a**; however, its activity is still in the micromolar range. Interestingly, the replacement of benzylic –CH₂ in **10b** with –C=O has drastically improved ChE inhibition activity (compound **10c**²⁰). This simple variation of –CH₂ vs –C=O impacts AChE inhibition by 20-fold and BChE inhibition by 10-fold. To understand the significantly different ChE inhibition by **10b** and **10c**, the docking with AChE was compared (Figure 3B,C). The –C=O in **10c** participates in

two vital H-bonding interactions with Phe 295 and Arg 296 residues at PAS. These interactions are not present in **10b**. Removal of –C=O from **10c** also results in a slight shift in the naphthyl position in the active site, with less tight π – π stacking with Trp 286. These vital differences in interactions of **10b** vs **10c** could be accounting for their different ChE inhibition activities.

The naphthyl derivative with the 4 F-benzyl moiety, **7av**, is the most active dual AChE/BChE inhibitor with IC_{50} values of 176 and 370 nM, respectively. The compound **7av** also exhibits 60 and 85% inhibition of self-induced A β 42-aggregation at 5 and 10 μM , respectively.

2.5. Enzyme Kinetics and Molecular Docking of Dual AChE/BChE Inhibitor 7av. To understand the type of inhibition and mode of interaction of **7av** with ChEs, enzyme kinetics and in silico studies were performed. Based on the Lineweaver–Burk double reciprocal plot, compound **7av** inhibits AChE in a non-competitive manner with an inhibition rate constant (k_i) of 0.046 μM (Figure 4A). The in silico docking of **7av** with AChE [Protein Data Bank (PDB) ID: 4EY7] further supported the non-competitive mode of inhibition. The compound **7av** occupies an active-site gorge and is engaged in various hydrophobic interactions with both PAS and CAS domain residues of the AChE protein (Figure

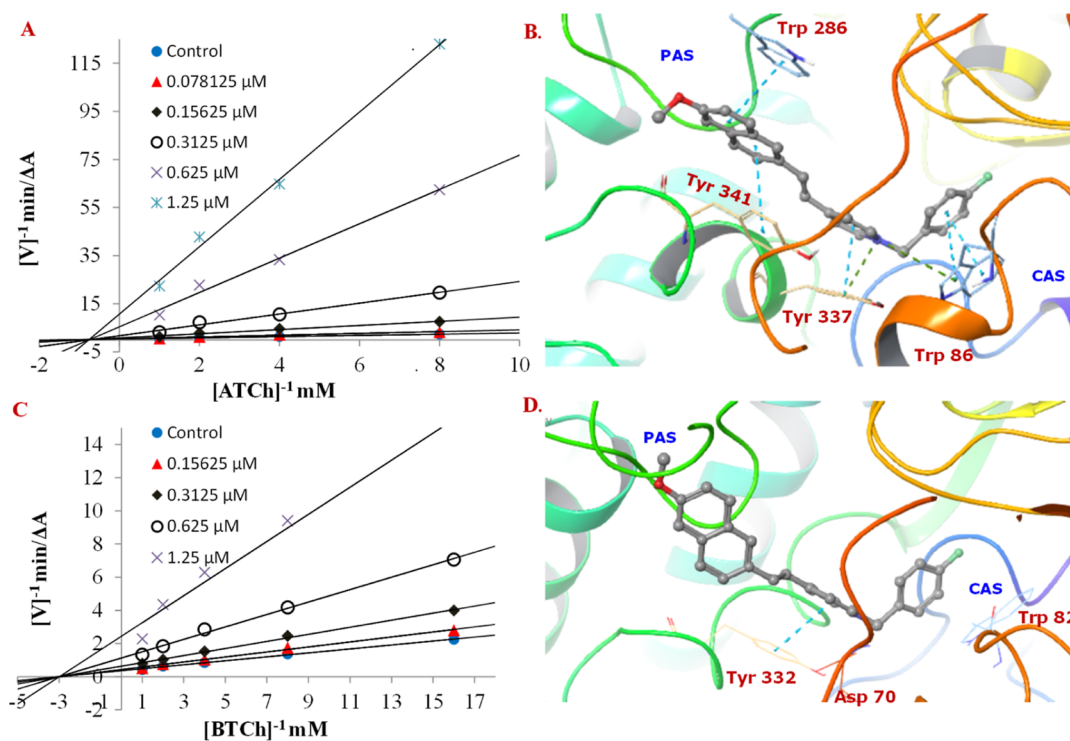


Figure 4. Enzyme kinetics and docking studies of **7av** with AChE and BChE enzymes. (A) LB plot indicating rHuAChE inhibition by **7av** and (B) interaction of **7av** with the hAChE active site. (C) LB plot for eqBChE inhibition by **7av** and (D) interactions of **7av** with the BChE active site. The abbreviations ATCh and BTCh denote acetylcholine and butyrylcholine, respectively.

4B). The naphthalene ring is oriented toward the PAS, while the *N*-benzyl moiety faces the CAS. In the PAS region, the naphthalene moiety stacks with Trp 286, while in the CAS region, the quaternary nitrogen constructs a cation- π interaction with Tyr 337 and Trp 86. Furthermore, the *N*-benzyl moiety reproduces a π - π stacking interaction with Trp 86. The nitrogen of the pyridinium ring displays a π -cation interaction with Tyr 337 and Trp 86 residues of the anionic subsite at the CAS. The eqBChE inhibition is also non-competitive, with a rate constant (k_i) of $0.115 \mu\text{M}$ (Figure 4C). The docking study validated the kinetic study results. The compound **7av** accommodates the active site with pyridinium ring stacking with Tyr 332 of PAS of BChE (Figure 4D). The elongated structure of the ligand allowed it to occupy the entire active-site gorge.

2.6. Molecular Dynamics Simulation. In the quest to find the stability of the protein-ligand (PL) complex, we performed molecular dynamics (MD) studies on the ligand **7av** with two protein systems hAChE (PDB ID: 4EY7) and hBChE (PDB: 6EP4). Initially, we performed the root mean square deviation (RMSD) analysis to foresee if there are any perturbations upon ligand binding within the protein cavity. The analysis revealed that both proteins remained almost stable throughout the simulation duration of 100 ns. However, a slight fluctuation for hAChE and hBChE in the range of 5.6–1.8 and 1.25–3.5 Å, respectively, occurred (Figures 5A and 6A). Second, a similar stable pattern was observed for the ligand **7av** throughout the simulation duration. Nevertheless, a little drift around 85 ns was observed in ligand RMSD in the case of hAChE (Figure 5A). Next, we performed root mean square fluctuation (RMSF) analysis to forecast perturbations that occur in the protein chain throughout the simulation upon ligand binding and lead to a plausibly unstable PL complex.

The protein RMSF for hAChE analysis revealed that the fluctuations were observed in the backbone residues of Thr 109 (3.1 Å), Gly 263 (4.8 Å), and Trp 385 (2.4 Å) (Figure 5B). Furthermore, the P-L contact diagram revealed that residual amino acids Trp 86, Trp 286, Tyr 337, and Tyr 341 were involved in the interactions with **7av** (Figure 5D). The major interaction (86%) was observed with the Trp 86 residue that was involved in the π - π stacking with the aromatic ring of **7av**. A similar interaction (π - π stacking) was observed with the Trp 286 residue (50%) and Tyr 341 residue (79%). Residues Trp 86 (30%) and Tyr 341 (60%) besides π - π stacking were also involved in the π -cationic interaction with Tyr 337 (38%), allowing the stability through the simulation time, as shown in Figure 5D. Moreover, Phe 338 is also involved in hydrophobic interactions over 80% of simulation that also aids in **7av**-AChE complex stabilization.

Next, the protein RMSF analysis for hBChE revealed the fluctuations over the backbone residues 250–300 (1.6 Å) and 350–400 (2 Å), as portrayed in Figure 6B. Furthermore, the P-L contact diagram illustrated that the Asp 70 residue was involved in the ionic interaction (56%) with nitrogen present in the heterocyclic ring of the **7av**, while the Tyr 332 residue was found to be involved in the π - π stacking (42%) with the aromatic ring, allowing the stability to PL complex through the simulation time. Moreover, 40% of the simulation was shown by hydrophobic interaction involving Trp 82, Pro 285, Tyr 430, and Tyr 440 residues aiding in additional complex stabilization (Figure 6D). The time-stamp analysis of both complexes is shown in the Supporting Information (Figures S54 and S55). Notably, most of the interactions found during the docking study (Figure 4B,D) were retained after 100 ns MD simulation, indicating both PL complexes' stable nature.

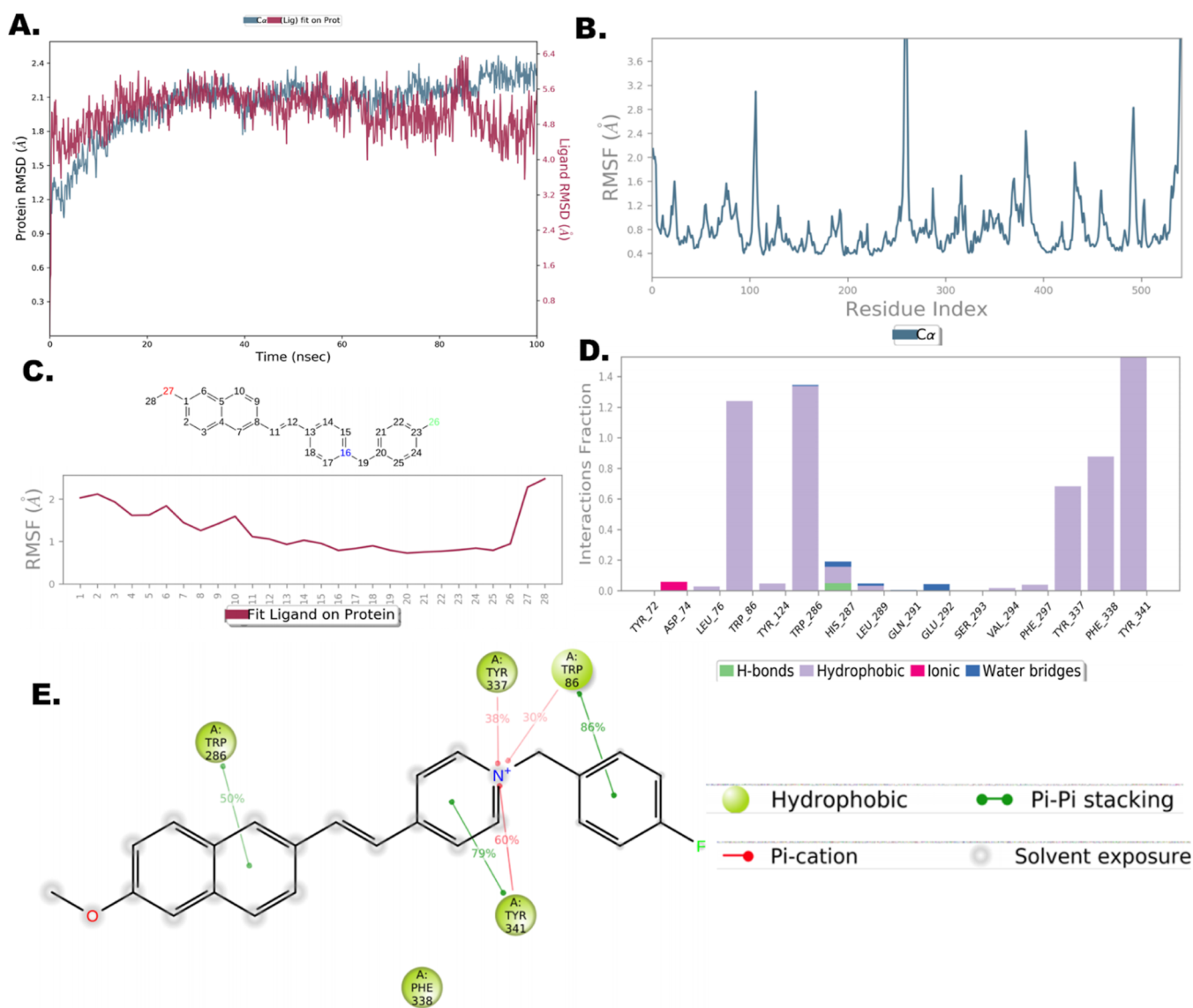


Figure 5. MD simulation of the 7av-hAChE complex. (A) RMSD plot protein–ligand interaction graph of hAChE; (B) RMSF of protein hAChE; (C) RMSF of the ligand; and (D) protein–ligand contact histogram. (E) 2D ligand–protein interaction.

2.7. Cytotoxicity of 7av in Cell Lines. The toxicity of 7av in J774A.1 cells and primary astrocytes was assessed for 48 h incubation time. Results are shown in Figure 7. Astrocytes are the major glial cells in the central nervous system and are involved in regulating various processes in the brain. These cells along with murine macrophages (J774A.1 cells) are used as model systems to study neuroinflammation. Therefore, cytotoxicity was assessed in these cells. The concentrations of 7av from 0.78 to 100 μM were tested, and it was found that the test compound reduces the cell viability in both cell lines. The compound is comparatively less toxic in primary astrocytes; however, its GI_{50} in both cell types is $\sim 6.25 \mu\text{M}$. The compound 7av was further tested for its effect on neuroinflammation via measuring the IL-1 β levels against nigericin-induced NLRP3 inflammasome activation; however, no statistically significant effect was observed.

The pyridinium compound, 7av, has a CLogP of 1.5, primarily because of the pyridinium salt. The investigation of its blood–brain barrier (BBB) permeability via PAMPA assay⁴¹ also revealed its low BBB permeability ($P_e < 3.0 \times 10^{-6}$ cm/s). However, pyridinyl compounds, e.g., pralidoxime

and obidoxime, are known to reach the brain as their pharmacokinetic studies have shown that BBB is not entirely impermeable to quaternary pyridinium compounds.⁴² Thus, a detailed pharmacokinetic study for 7av would be required to understand its brain exposure and the permeation mechanism.

3. CONCLUSIONS

The “pyridinium styryl” scaffold identified via e-pharmacophore modeling was investigated in detail for lead optimization toward identifying a dual ChE inhibitor. The synthesis of fifty-three *N*-benzyl pyridinium styryl derivatives followed by their in vitro ChE inhibition assays led to the identification of 7av (SB-1436) as a dual AChE and BChE inhibitor showing half-maximal inhibitory concentration values of 0.176 and 0.37 μM , respectively. The enzyme kinetics and docking studies have demonstrated that SB-1436 exhibits a non-competitive mode of inhibition for both AChE and BChE with k_i values of 0.046 and 0.115 μM , respectively. In addition to its dual ChE inhibition, it also stops the self-aggregation of the A β 42 peptide. The SAR studies on pyridinium styryls indicate that

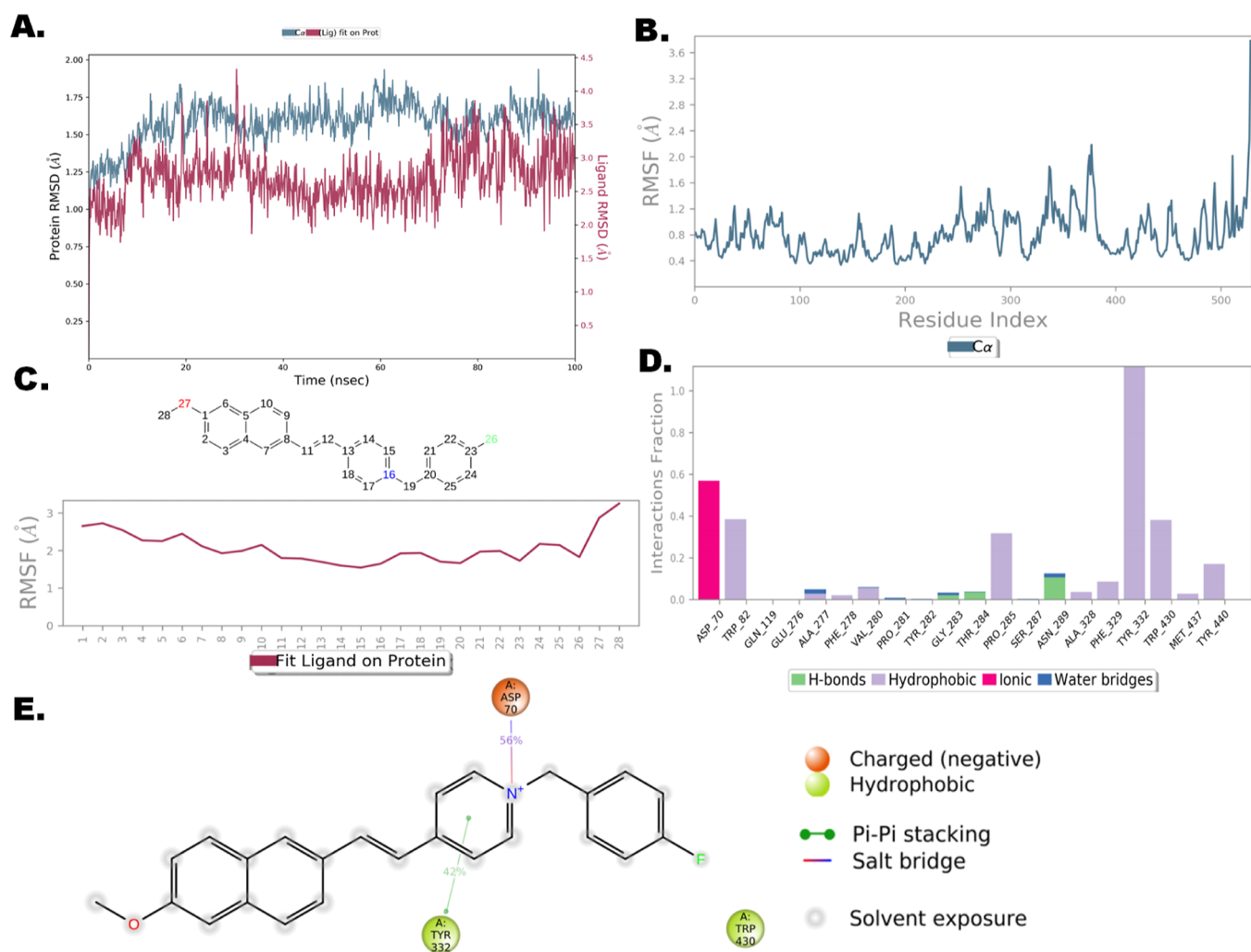


Figure 6. MD simulation of the 7av-hBChE complex. (A) RMSD plot protein–ligand interaction graph of hBChE; (B) RMSF of protein hBChE; (C) RMSF of ligand; and (D) protein–ligand contacts histogram. (E) 2D ligand–protein interaction.

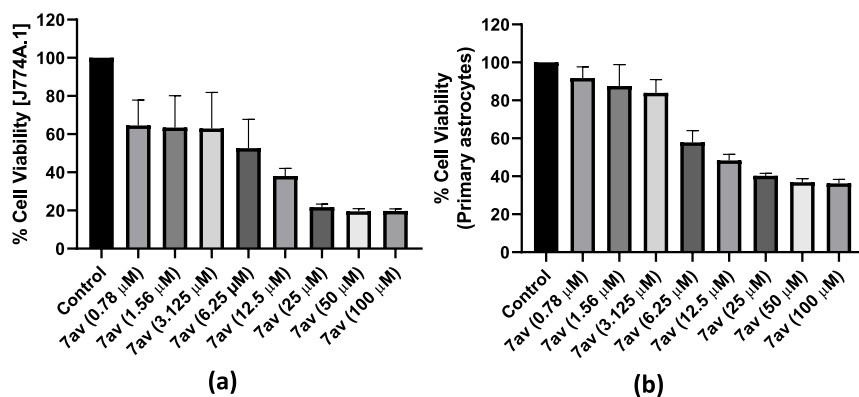


Figure 7. Effect of 7av on the cell viability of J774.1 cells (a) and primary astrocytes (b).

chloro or fluoro on the benzylic ring (ring C) boosts the BChE inhibition activity. The presence of naphthyl ring vs. phenyl (ring A) also helps in a drastic boost in BChE inhibition potency. Further replacement of the “pyridinium” ring (ring B) with non-quaternary “piperidine” is still able to maintain a dual AChE/BChE inhibition potency. These SAR studies provide vital insights into further ChE-targeted medicinal chemistry on this scaffold. Overall, the results presented herein advocate the

detailed preclinical investigation of the identified dual ChE inhibitor, 7av.

4. EXPERIMENTAL SECTION

4.1. General. All chemicals were purchased from Sigma-Aldrich and TCI Companies and were used as such as received without further purifications. The instruments used to record

the analytical data, such as ^1H , ^{13}C , IR, and melting point data, were the same as the previous work.⁴³

4.2. General Procedure for the Preparation of Benzyl Alcohols, 2a–k. To the solution of aryl aldehyde, 1a–k, in methanol was added slowly NaBH_4 under an ice bath with continuous stirring. The mixture was concentrated on a rotary evaporator and partitioned between ethyl acetate and water. The ethyl acetate layer was evaporated on a vacuo rotavapor to dryness to obtain the corresponding benzyl alcohols, 2a–j, which were used as such for the next step.

4.3. General Procedure for the Preparation of Benzyl Bromides, 3a–k. To a solution of *N*-bromosuccinamide in methylene chloride was slowly added PPh_3 at 0 °C with continuous stirring. The resulting mixture was refluxed at 60 °C for 15 min. The reaction mixture was cooled to room temperature. Benzyl alcohol was added to the cooled reaction mixture, and it was then refluxed at 60 °C for 30 min. The reaction mixture was concentrated to dryness, and the obtained product was used as such for the next step.

4.4. General Procedure for the Preparation of Benzyltriphenylphosphonium Bromides, 4a–j, and ((6-Methoxynaphthalen-2-yl)methyl)-triphenylphosphonium Bromide (4k). To a solution of benzyl bromide in THF was added PPh_3 (1.2 equiv) slowly at 0 °C with continuous stirring. The resulting mixture was refluxed at 85 °C for 2 h. A white solid is formed, indicating the formation of Wittig salt. The reaction mixture was allowed to cool to room temperature and then filtered. The solid residue was washed with ethyl acetate or THF, dried under vacuum, and used for the next step.

4.5. General Procedure for the Preparation of (E)-4-Styrylpyridines, 6a–k. To the solution of triphenylphosphine halide salts 4a–k (2 mmol) in dry THF, potassium *tert*-butoxide (2.5 mmol) was added at room temperature. The resulting mixture was refluxed for 30 min. The color of the reaction mixture turned orange after which it was allowed to cool to room temperature. The pyridine aldehyde 5 (2 mmol) was added, and the resulting reaction mixture was refluxed at 80 °C for 30 min. THF was evaporated on a vacuo rotavapor, and the resultant solid mass was partitioned between ethyl acetate and water. The ethyl acetate layer was dried over anhydrous sodium sulfate, which was further evaporated on a rotary evaporator to obtain the crude product. Purification was done using routine silica gel (mesh 100–200) column chromatography using ethyl acetate–hexane as a mobile phase to obtain (E)-4-styrylpyridine 6a–k in 80–95% yield.

4.6. General Procedure for the Preparation of *N*-Benzyl Pyridinium Salts, 7a–7ax. To the solution of (E)-4-styrylpyridines, 6a–k (0.5 mmol) in ACN (10 mL) was added benzyl halides (0.5 mmol), and the resulting mixture was stirred at 80 °C for 1 h. The formation of white/yellow precipitates was seen in the reaction mixture. The precipitates were filtered and washed with acetone (10 mL \times 3). The resulting residue was dried to obtain the desired *N*-benzyl pyridinium styryls, 7a–7ax, in 85–95% yield.

4.6.1. (E)-1-Benzyl-4-(3,5-dimethoxystyryl)pyridin-1-ium bromide (7a). Yield: 88%; yellow solid; mp 250–252 °C; IR (ν_{max}): 3416, 3034, 2920, 1740, 1622, 1554, 1495, 1470, 1455, 1427, 1336, 1305, 1286, 1207, 1056, 972 cm^{-1} ; ^1H NMR (400 MHz, CD_3OD): δ 8.78 (d, J = 6.8 Hz, 2H), 8.10 (d, J = 6.8 Hz, 2H), 7.76 (d, J = 16.3 Hz, 1H), 7.42–7.32 (m, 6H), 6.82 (s, 2H), 6.51 (s, 1H), 5.66 (s, 2H), 3.75 (s, 6H); ^{13}C NMR (126 MHz, CDCl_3): δ 165.33, 158.45, 147.85, 146.06, 140.85,

137.54, 133.46, 133.24, 132.51, 128.09, 126.78, 109.84, 106.47, 67.13, 58.52. ESI-MS m/z : 332.0 $[\text{M} - \text{Br}]^+$; HR-ESIMS m/z : 332.1654 calcd for $\text{C}_{22}\text{H}_{22}\text{NO}_2^+$ (332.1651).

4.6.2. (E)-4-(3,5-Dimethoxystyryl)-1-(2-methylbenzyl)pyridin-1-ium bromide (7b). Yield: 91%; yellow solid; mp 261–263 °C; IR (ν_{max}): 3584, 2919, 1641, 1617, 1592, 1514, 1461, 1426, 1257, 1063, 986 cm^{-1} ; ^1H NMR (400 MHz, CD_3OD): δ 8.63 (d, J = 6.8 Hz, 2H), 8.09 (d, J = 6.8 Hz, 2H), 7.77 (d, J = 16.3 Hz, 1H), 7.35–7.27 (m, 3H), 6.81 (d, J = 2.1 Hz, 2H), 6.49 (d, J = 2.0 Hz, 1H), 5.71 (s, 2H), 3.74 (s, 6H) 2.24 (s, 3H); ^{13}C NMR (126 MHz, $\text{DMSO}-d_6$): δ 161.27, 153.76, 141.69, 137.54, 137.33, 133.02, 131.38, 129.75, 129.42, 127.19, 124.69, 124.39, 106.60, 103.03, 61.01, 55.92, 19.29. ESI-MS m/z : 346.0 $[\text{M} - \text{Br}]^+$; HR-ESIMS m/z : 346.1808 calcd for $\text{C}_{23}\text{H}_{24}\text{NO}_2^+$, (346.1807).

4.6.3. (E)-4-(3,5-Dimethoxystyryl)-1-(2-chlorobenzyl)pyridin-1-ium chloride (7c). Yield: 87%; yellow solid; mp 250–252 °C; IR (ν_{max}): 3446, 3383, 3013, 2964, 2920, 2850, 1700, 1695, 1642, 1624, 1586, 1472, 1451, 1428, 1356, 1331, 1316, 1294, 1283, 979 cm^{-1} ; ^1H NMR (400 MHz, CD_3OD): δ 8.71 (d, J = 6.8 Hz, 2H), 8.09 (d, J = 6.8 Hz, 2H), 7.78 (d, J = 16.3 Hz, 1H), 7.53–7.39 (m, 5H), 6.81 (d, J = 2.1 Hz, 2H), 6.48 (t, J = 2.1 Hz, 1H), 5.79 (s, 2H), 3.74 (s, 6H); ^{13}C NMR (126 MHz, CD_3OD): δ 161.37, 154.72, 144.07, 142.34, 136.92, 134.36, 132.00, 131.64, 130.79, 130.26, 128.01, 124.02, 122.85, 105.95, 102.64, 60.92, 54.62. ESI-MS m/z : 366.0 $[\text{M} - \text{Cl}]^+$; HR-ESIMS m/z : 366.1261 calcd for $\text{C}_{22}\text{H}_{21}\text{ClNO}_2^+$, (366.1261).

4.6.4. (E)-4-(3,5-Dimethoxystyryl)-1-(3-chlorobenzyl)pyridin-1-ium chloride (7d). Yield: 90%; yellow solid; mp 149–151 °C; IR (ν_{max}): 3387, 3038, 2922, 2847, 1658, 1641, 1620, 1594, 1456, 1427, 1354, 1289, 1208, 1159, 973 cm^{-1} ; ^1H NMR (400 MHz, CD_3OD): δ 8.77 (d, J = 6.7 Hz, 2H), 8.09 (d, J = 6.8 Hz, 2H), 7.78 (d, J = 16.3 Hz, 1H), 7.49 (s, 1H), 7.39–7.32 (m, 4H), 6.81 (d, J = 2.1 Hz, 2H), 6.48 (s, 1H), 5.64 (s, 2H), 3.74 (s, 6H); ^{13}C NMR (126 MHz, CD_3OD): δ 161.36, 154.71, 143.90, 142.29, 136.91, 135.62, 135.02, 130.92, 129.64, 128.61, 126.97, 124.31, 122.88, 105.99, 102.61, 62.38, 54.68. ESI-MS m/z : 366.0 $[\text{M} - \text{Cl}]^+$; HR-ESIMS m/z : 366.1262 calcd for $\text{C}_{22}\text{H}_{21}\text{ClNO}_2^+$ (366.1261).

4.6.5. (E)-4-(3,5-Dimethoxystyryl)-1-(4-chlorobenzyl)pyridin-1-ium chloride (7e). Yield: 93%; yellow solid; IR (ν_{max}): 3387, 2921, 2850, 1620, 1592, 1556, 1517, 1454, 1425, 1351, 1287, 1208, 1159, 1095, 975 cm^{-1} ; ^1H NMR (400 MHz, CD_3OD): δ 8.75 (d, J = 6.8 Hz, 2H), 8.09 (d, J = 6.7 Hz, 2H), 7.77 (d, J = 16.3 Hz, 1H), 7.40–7.33 (m, 5H), 6.81 (d, J = 2.1 Hz, 2H), 6.49 (t, J = 2.0 Hz, 1H), 5.63 (s, 2H), 3.74 (s, 6H); ^{13}C NMR (126 MHz, CD_3OD): δ 161.37, 154.60, 143.88, 142.21, 136.92, 135.53, 132.35, 130.32, 129.37, 124.23, 122.86, 105.93, 102.60, 62.28, 54.61. ESI-MS m/z : 366.0 $[\text{M} - \text{Cl}]^+$; HR-ESIMS m/z : 366.1270 calcd for $\text{C}_{22}\text{H}_{21}\text{ClNO}_2^+$ (366.1261).

4.6.6. (E)-4-(3,5-Dimethoxystyryl)-1-(2-fluorobenzyl)pyridin-1-ium bromide (7f). Yield: 89%; yellow solid; mp 257–259 °C; IR (ν_{max}): 3416, 3010, 2921, 2849, 1625, 1562, 1518, 1492, 1356, 1285, 1257, 1214, 1197, 1181, 977 cm^{-1} ; ^1H NMR (400 MHz, CD_3OD): δ 8.75 (d, J = 6.3 Hz, 2H), 8.09 (d, J = 6.2 Hz, 2H), 7.77 (d, J = 16.2 Hz, 1H), 7.53–7.24 (m, 5H), 6.81 (br s, 2H), 6.48 (br s, 1H), 5.73 (s, 2H), 3.74 (s, 6H); ^{13}C NMR (126 MHz, CD_3OD): δ 161.40, 154.74, 143.97, 142.34, 132.35, 132.28, 131.31, 125.18, 124.12, 122.81, 120.81, 120.69, 115.96, 115.80, 105.92, 102.56, 57.64, 54.57.

ESI-MS m/z : 350.0 $[M - Br]^+$; HR-ESIMS m/z : 350.1558 calcd for $C_{22}H_{21}FNO_2^+$ (350.1556).

4.6.7. (E)-4-(3,5-Dimethoxystyryl)-1-(4-fluorobenzyl)pyridin-1-ium chloride (7g). Yield: 90%; white solid; mp 220–222 °C; IR (ν_{max}): 3359, 2839, 1618, 1591, 1528, 1470, 1367, 1286, 1224, 1207, 1158, 1067, 925 cm^{-1} ; 1H NMR (400 MHz, CD_3OD): δ 8.75 (d, $J = 6.8$ Hz, 2H), 8.08 (d, $J = 6.8$ Hz, 2H), 7.77 (d, $J = 16.3$ Hz, 1H), 7.49–7.12 (m, 5H), 6.80 (d, $J = 2.1$ Hz, 2H), 6.49 (t, $J = 2.1$ Hz, 1H), 5.63 (s, 2H), 3.74 (s, 6H); ^{13}C NMR (126 MHz, CD_3OD): δ 164.50, 162.52, 161.36, 154.52, 143.78, 142.13, 136.93, 131.12 ($^3J_{CF} = 8.8$ Hz), 129.68, 124.20, 122.86, 116.19 ($^2J_{CF} = 22.7$ Hz), 105.91, 102.58, 62.32, 54.60. ESI-MS m/z : 350.0 $[M - Cl]^+$; HR-ESIMS m/z : 350.1556 calcd for $C_{22}H_{21}FNO_2^+$ (350.1556).

4.6.8. (E)-4-(3,5-Dimethoxystyryl)-1-(2-nitrobenzyl)pyridin-1-ium bromide (7h). Yield: 93%; yellow solid; mp 251–253 °C; IR (ν_{max}): 3384, 2918, 2849, 1341, 1616, 1592, 1539, 1521, 1464, 1456, 1425, 1342, 1287, 1156, 973 cm^{-1} ; 1H NMR (400 MHz, CD_3OD): δ 8.70 (d, $J = 6.7$ Hz, 2H), 8.22 (d, $J = 8.1$ Hz, 1H), 8.12 (d, $J = 6.7$ Hz, 2H), 7.82–7.76 (m, 2H), 7.69 (t, $J = 7.8$ Hz, 1H), 7.43 (d, $J = 7.6$ Hz, 1H), 7.37 (d, $J = 16.3$ Hz, 1H), 6.82 (d, $J = 1.8$ Hz, 2H), 6.50 (s, 1H), 6.02 (s, 2H), 3.74 (s, 6H); ^{13}C NMR (126 MHz, $DMSO-d_6$): δ 161.27, 154.04, 148.30, 145.22, 142.03, 141.95, 137.51, 130.41, 124.85, 124.63, 124.32, 106.63, 103.10, 61.59, 55.93. ESI-MS m/z : 377.0 $[M - Br]^+$; HR-ESIMS m/z : 377.1505 calcd for $C_{22}H_{21}N_2O_4^+$ (377.1501).

4.6.9. (E)-4-(3,5-Dimethoxystyryl)-1-(4-nitrobenzyl)pyridin-1-ium bromide (7i). Yield: 95%; orange solid; mp 184–186 °C; IR (ν_{max}): 3356, 2921, 2349, 2334, 1616, 1555, 1517, 1469, 1347, 1205, 1161, 987 cm^{-1} ; 1H NMR (400 MHz, $DMSO-d_6$): δ 8.98 (d, $J = 6.4$ Hz, 2H), 8.18 (dd, $J = 10.1$, 7.8 Hz, 4H), 7.87 (d, $J = 16.3$ Hz, 1H), 7.65 (d, $J = 8.3$ Hz, 2H), 7.47 (d, $J = 16.3$ Hz, 1H), 6.83 (s, 2H), 6.50 (s, 1H), 5.82 (s, 2H), 3.70 (s, 6H); ^{13}C NMR (126 MHz, $DMSO-d_6$): δ 161.27, 154.04, 148.31, 145.21, 142.02, 141.95, 137.51, 130.40, 124.85, 124.63, 124.32, 106.63, 103.10, 61.60, 55.93. ESI-MS m/z : 377.0 $[M - Br]^+$; HR-ESIMS m/z : 377.1505 calcd for $C_{22}H_{21}N_2O_4^+$ (377.1501).

4.6.10. (E)-1-Benzyl-4-(3,4-dimethoxystyryl)pyridin-1-ium bromide (7j). Yield: 87%; yellow solid; mp 263–265 °C; IR (ν_{max}): 3328, 2948, 2869, 1703, 1626, 1558, 1522, 1421, 1401, 1223, 1188, 1150, 1128, 970 cm^{-1} ; 1H NMR (400 MHz, $DMSO-d_6$): δ 8.95 (d, $J = 6.8$ Hz, 2H), 8.11 (d, $J = 6.8$ Hz, 2H), 7.90 (d, $J = 16.2$ Hz, 1H), 7.45 (d, $J = 6.3$ Hz, 2H), 7.40–7.32 (m, 5H), 7.21 (dd, $J = 8.3$, 1.7 Hz, 1H), 6.99 (d, $J = 8.4$ Hz, 1H), 5.65 (s, 2H), 3.76 (s, 3H), 3.74 (s, 3H); ^{13}C NMR (101 MHz, $DMSO-d_6$): δ 154.20, 151.75, 149.56, 144.59, 142.17, 135.12, 129.70, 129.10, 128.43, 124.07, 123.86, 121.26, 112.20, 110.39, 62.54, 56.12, 56.08. ESI-MS m/z : 332.0 $[M - Br]^+$; HR-ESIMS m/z : 332.1651 calcd for $C_{22}H_{22}NO_2^+$ (332.1651).

4.6.11. (E)-4-(3,4-Dimethoxystyryl)-1-(2-methylbenzyl)pyridin-1-ium bromide (7k). Yield: 87%; yellow solid; mp 255–257 °C; IR (ν_{max}): 3356, 2936, 2858, 1622, 1598, 1517, 1497, 1422, 1223, 1175, 1126, 1022 cm^{-1} ; 1H NMR (400 MHz, $DMSO-d_6$): δ 8.76 (d, $J = 5.9$ Hz, 2H), 8.09 (d, $J = 5.9$ Hz, 2H), 7.89 (d, $J = 16.3$ Hz, 1H), 7.37 (d, $J = 16.2$ Hz, 1H), 7.32 (s, 1H), 7.27–7.17 (m, 4H), 7.05 (d, $J = 7.5$ Hz, 1H), 6.98 (d, $J = 8.4$ Hz, 1H), 5.69 (s, 2H), 3.75 (s, 3H), 3.73 (s, 3H), 2.21 (s, 3H); ^{13}C NMR (126 MHz, CD_3OD): δ 154.97, 152.08, 149.57, 143.52, 142.41, 137.37, 131.28, 131.24, 131.10, 129.81, 129.72, 128.23, 126.79, 123.45, 120.11, 111.39, 111.31,

110.20, 110.06, 61.05, 55.22, 55.08, 17.79. ESI-MS m/z : 346.0 $[M - Br]^+$; HR-ESIMS m/z : 346.1809 calcd for $C_{23}H_{24}NO_2^+$ (346.1807).

4.6.12. (E)-1-(2-Chlorobenzyl)-4-(3,4-dimethoxystyryl)pyridin-1-ium chloride (7l). Yield: 88%; yellow solid; mp 156–158 °C; IR (ν_{max}): 3352, 2927, 2856, 1632, 1586, 1477, 1423, 1236, 1184, 1022 cm^{-1} ; 1H NMR (400 MHz, CD_3OD): δ 8.63 (d, $J = 6.2$ Hz, 2H), 8.02 (d, $J = 6.2$ Hz, 2H), 7.80 (d, $J = 16.1$ Hz, 1H), 7.52–7.47 (m, 5H), 7.44–7.28 (m, 2H), 6.94 (d, $J = 8.4$ Hz, 1H), 5.75 (s, 2H), 3.81 (s, 3H), 3.80 (s, 3H); ^{13}C NMR (126 MHz, CD_3OD): δ 143.74, 142.67, 135.38, 133.82, 131.88, 131.61, 130.94, 130.28, 129.86, 129.45, 127.99, 127.12, 123.56, 123.35, 120.03, 111.30, 110.03, 60.70, 55.15, 55.10. ESI-MS m/z : 366.0 $[M - Cl]^+$; HR-ESIMS m/z : 366.1263 calcd for $C_{22}H_{21}ClNO_2^+$ (366.1261).

4.6.13. (E)-4-(3,4-Dimethoxystyryl)-1-(4-fluorobenzyl)pyridin-1-ium chloride (7m). Yield: 90%; yellow solid; mp 157–159 °C; IR (ν_{max}): 3348, 2950, 2866, 1622, 1598, 1533, 1494, 1453, 1241, 1182, 1123, 1056 cm^{-1} ; 1H NMR (400 MHz, CD_3OD): δ 8.68 (d, $J = 6.4$ Hz, 2H), 8.02 (d, $J = 6.4$ Hz, 2H), 7.79 (d, $J = 16.2$ Hz, 1H), 7.46 (dd, $J = 7.9$, 5.4 Hz, 2H), 7.27 (br s, 2H), 7.24–7.19 (m, 2H), 6.94 (d, $J = 8.3$ Hz, 2H), 5.60 (s, 2H), 3.81 (s, 3H), 3.80 (s, 3H); ^{13}C NMR (126 MHz, CD_3OD): δ 164.45 ($^1J_{CF} = 248$ Hz), 154.91, 151.93, 149.50, 143.46, 142.33, 131.07 ($^3J_{CF} = 8.8$ Hz), 129.83, 128.23, 123.57, 123.46, 120.11, 116.16 ($^2J_{CF} = 21.4$ Hz), 111.31, 110.07, 62.09, 55.18, 55.10. ESI-MS m/z : 350.0 $[M - Cl]^+$; HR-ESIMS m/z : 350.1555 calcd for $C_{22}H_{21}FNO_2^+$ (350.1556).

4.6.14. (E)-4-(3,4-Dimethoxystyryl)-1-(4-nitrobenzyl)pyridin-1-ium bromide (7n). Yield: 88%; yellow solid; mp 199–201 °C; IR (ν_{max}): 3336, 2955, 2893, 1629, 1597, 1522, 1498, 1443, 1235, 1183, 1154, 1106, 1031, 956 cm^{-1} ; 1H NMR (400 MHz, CD_3OD): δ 8.90 (d, $J = 6.8$ Hz, 2H), 8.41 (d, $J = 8.7$ Hz, 2H), 8.25 (d, $J = 6.8$ Hz, 2H), 8.01 (d, $J = 16.2$ Hz, 1H), 7.78 (d, $J = 8.6$ Hz, 2H), 7.47–7.340 (m, 3H), 7.13 (d, $J = 8.4$ Hz, 1H), 5.95 (s, 2H), 4.00 (s, 3H), 3.98 (s, 3H); ^{13}C NMR (126 MHz, $DMSO-d_6$): δ 154.55, 151.82, 149.57, 148.28, 144.89, 142.50, 142.15, 130.34, 128.44, 124.64, 124.17, 123.96, 121.25, 112.22, 110.47, 61.39, 56.14, 56.11. ESI-MS m/z : 377.0 $[M - Br]^+$; HR-ESIMS m/z : 377.1507 calcd for $C_{22}H_{21}N_2O_4^+$ (377.1501).

4.6.15. (E)-1-(2-Methylbenzyl)-4-(3,4,5-trimethoxystyryl)pyridin-1-ium bromide (7o). Yield: 86%; yellow solid; mp 225–227 °C; IR (ν_{max}): 3420, 3040, 2921, 2849, 1636, 1581, 1537, 1466, 1422, 1355, 1337, 1276, 1211, 1152 cm^{-1} ; 1H NMR (400 MHz, CD_3OD): δ 8.60 (d, $J = 6.8$ Hz, 2H), 8.05 (d, $J = 6.8$ Hz, 2H), 7.79 (d, $J = 16.2$ Hz, 1H), 7.28 (m, 5H), 6.98 (br s, 2H), 5.70 (s, 2H), 3.82 (s, 6H), 3.72 (s, 3H), 2.24 (s, 3H); ^{13}C NMR (126 MHz, CD_3OD): δ 154.64, 154.60, 153.55, 153.53, 143.66, 142.16, 142.13, 137.42, 131.18, 131.12, 130.94, 129.87, 129.81, 126.82, 123.81, 123.79, 121.79, 105.71, 105.62, 61.19, 59.87, 55.44, 55.41, 17.83. ESI-MS m/z : 376.0 $[M - Br]^+$; HR-ESIMS m/z : 376.1910 calcd for $C_{24}H_{26}NO_3^+$ (376.1913).

4.6.16. (E)-1-(2-Chlorobenzyl)-4-(3,4,5-trimethoxystyryl)pyridin-1-ium chloride (7p). Yield: 88%; yellowish solid; mp 210–212 °C; IR (ν_{max}): 3368, 2954, 1616, 1580, 1503, 1466, 1421, 1359, 1276, 1241, 1182, 1055 cm^{-1} ; 1H NMR (400 MHz, CD_3OD): δ 8.68 (d, $J = 6.6$ Hz, 2H), 8.06 (d, $J = 6.7$ Hz, 2H), 7.80 (d, $J = 16.2$ Hz, 1H), 7.51–7.47 (m, 2H), 7.45–7.39 (m, 2H), 7.31 (d, $J = 16.2$ Hz, 1H), 6.98 (s, 2H), 5.77 (s, 2H), 3.82 (s, 6H), 3.73 (s, 3H); ^{13}C NMR (126 MHz, CD_3OD): δ 154.89, 153.57, 143.97, 142.42, 134.50, 131.90, 131.63, 130.85,

130.82, 130.28, 128.00, 123.68, 121.72, 105.62, 60.82, 59.84, 55.34. ESI-MS m/z : 396.0 $[M - Cl]^+$; HR-ESIMS m/z : 396.1366 calcd for $C_{23}H_{23}ClNO_3^+$ (396.1366).

4.6.17. (*E*)-1-(4-Fluorobenzyl)-4-(3,4,5-trimethoxystyryl)pyridin-1-ium chloride (**7q**). Yield: 90%; yellow solid; mp 182–184 °C; IR (ν_{max}): 3416, 2918, 2848, 1616, 1641, 1581, 1510, 1467, 1423, 1356, 1327, 1228, 1151, 1125, 997 cm^{-1} ; 1H NMR (400 MHz, CD_3OD): δ 8.73 (d, $J = 6.7$ Hz, 2H), 8.05 (d, $J = 6.7$ Hz, 2H), 7.78 (d, $J = 16.2$ Hz, 2H), 7.49–7.45 (m, 2H), 7.30 (d, $J = 16.2$ Hz, 2H), 6.98 (s, 2H), 5.62 (s, 2H), 3.81 (s, 6H), 3.72 (s, 3H); ^{13}C NMR (126 MHz, CD_3OD): δ 153.61, 143.66, 142.26, 130.94, 123.90, 121.72, 116.20, 116.03, 105.72, 62.30, 59.85, 55.39. ESI-MS m/z : 380.0 $[M - Cl]^+$; HR-ESIMS m/z : 380.1664 calcd for $C_{23}H_{23}FNO_3^+$ (380.1662).

4.6.18. (*E*)-1-(2-Nitrobenzyl)-4-(3,4,5-trimethoxystyryl)pyridin-1-ium bromide (**7r**). Yield: 91%; yellow solid 217–219 °C; IR (ν_{max}): 3386, 3096, 2928, 2855, 1620, 1594, 1558, 1471, 1427, 1367, 1354, 1289, 1208, 1159, 1097, 1082, 1068, 1057, 973 cm^{-1} ; 1H NMR (400 MHz, CD_3OD): δ 8.67 (d, $J = 6.8$ Hz, 2H), 8.23 (d, $J = 8.1$ Hz, 1H), 8.08 (d, $J = 6.7$ Hz, 2H), 7.82–7.69 (m, 4H), 7.42 (d, $J = 7.6$ Hz, 1H), 7.33 (d, $J = 16.2$ Hz, 1H), 6.99 (s, 1H), 6.00 (s, 2H), 3.82 (s, 6H), 3.73 (s, 3H); ^{13}C NMR (126 MHz, CD_3OD): δ 154.96, 153.56, 148.08, 144.13, 142.46, 140.42, 134.69, 131.94, 131.05, 130.89, 127.93, 125.86, 123.67, 121.77, 105.65, 60.24, 59.84, 55.37. ESI-MS m/z : 407.0 $[M - Br]^+$; HR-ESIMS m/z : 407.1613 calcd for $C_{23}H_{23}N_2O_5^+$ (407.1607).

4.6.19. (*E*)-1-(4-Nitrobenzyl)-4-(3,4,5-trimethoxystyryl)pyridin-1-ium bromide (**7s**). Yield: 93%; Red solid; mp 200–202 °C; IR (ν_{max}): 3357, 2924, 2853, 1612, 1516, 1456, 1419, 1377, 1345, 1328, 1277, 1241, 1210, 1155, 962 cm^{-1} ; 1H NMR (400 MHz, $DMSO-d_6$): δ 8.96 (d, $J = 5.7$ Hz, 2H), 8.20 (d, $J = 8.4$ Hz, 2H), 8.13 (d, $J = 6.0$ Hz, 2H), 7.90 (d, $J = 16.2$ Hz, 1H), 7.66 (d, $J = 8.2$ Hz, 2H), 7.44 (d, $J = 16.2$ Hz, 1H), 7.00 (s, 2H), 5.81 (s, 2H), 3.75 (s, 6H), 3.62 (s, 3H); ^{13}C NMR (101 MHz, $DMSO-d_6$): δ 155.08, 149.77, 146.49, 143.72, 143.35, 132.53, 131.80, 126.05, 125.91, 124.36, 107.85, 63.06, 62.12, 57.99. ESI-MS m/z : 407.0 $[M - Br]^+$; HR-ESIMS m/z : 407.1607 calcd for $C_{23}H_{23}N_2O_5^+$ (407.1607).

4.6.20. (*E*)-1-Benzyl-4-(4-methoxystyryl)pyridin-1-ium bromide (**7t**). Yield: 94%; yellow solid; mp 214–216 °C; IR (ν_{max}): 3428, 3032, 2960, 2925, 2860, 2363, 1615, 1596, 1519, 1436, 1393, 1289, 1258, 1157, 1042, 985 cm^{-1} ; 1H NMR (400 MHz, CD_3OD): δ 8.69 (d, $J = 6.9$ Hz, 2H), 8.02 (d, $J = 6.9$ Hz, 2H), 7.81 (d, $J = 16.2$ Hz, 1H), 7.61 (m, 3H), 7.39–7.36 (m, 5H), 6.92 (d, $J = 8.8$ Hz, 2H), 5.61 (s, 2H), 3.76 (s, 3H). ^{13}C NMR (126 MHz, CD_3OD): δ 162.23, 154.95, 143.55, 142.11, 133.73, 130.05, 129.45, 129.28, 128.54, 127.77, 123.54, 119.83, 114.29, 62.96, 54.61. ESI-MS m/z : 302.0 $[M - Br]^+$; HR-ESIMS m/z : 302.1548 calcd for $C_{21}H_{20}NO^+$ (302.1545).

4.6.21. (*E*)-4-(4-Methoxystyryl)-1-(2-fluorobenzyl)pyridin-1-ium bromide (**7u**). Yield: 88%; yellow solid; mp 222–227 °C; IR (ν_{max}): 3405, 3034, 2922, 2351, 1618, 1595, 1572, 1556, 1517, 1493, 1468, 1425, 1329, 1308, 1259, 1214, 1024, 988 cm^{-1} ; 1H NMR (400 MHz, CD_3OD): δ 8.78 (d, $J = 6.8$ Hz, 2H), 8.12 (d, $J = 6.9$ Hz, 2H), 7.92 (d, $J = 16.2$ Hz, 1H), 7.71 (d, $J = 8.8$ Hz, 2H), 7.61–7.50 (m, 5H), 7.02 (d, $J = 8.7$ Hz, 2H), 5.79 (s, 2H), 3.86 (s, 3H); ^{13}C NMR (126 MHz, CD_3OD): δ 162.32 ($J_{CF} = 259$ Hz), 155.22, 143.64, 142.38, 132.27, 132.20, 131.25, 130.31, 130.07, 127.75, 127.11, 125.18, 125.15, 123.49, 120.76, 119.79, 115.93 ($J_{CF} = 20$ Hz), 114.31,

114.18, 57.39, 54.61. ESI-MS m/z : 320.0 $[M - Cl]^+$; HR-ESIMS m/z : 320.1450 calcd for $C_{21}H_{19}FNO^+$ (320.1451).

4.6.22. (*E*)-4-(4-Methoxystyryl)-1-(2-nitrobenzyl)pyridin-1-ium bromide (**7v**). Yield: 87%; yellow solid; mp 205–207 °C; IR (ν_{max}): 3425, 2928, 2836, 1645, 1522, 1452, 1345, 1256, 1157, 1022 cm^{-1} ; 1H NMR (400 MHz, CD_3OD): δ 8.98 (d, $J = 6.4$ Hz, 1H), 8.74 (d, $J = 6.6$ Hz, 2H), 8.32–8.30 (m, 1H), 8.20 (d, $J = 6.3$ Hz, 2H), 7.90–7.60 (m, 5H), 7.55 (dd, $J = 21.7$, 7.4 Hz, 1H), 7.02 (d, $J = 8.6$ Hz, 1H), 6.21 (s, 1H), 6.09 (s, 2H), 3.87 (s, 3H); ^{13}C NMR (126 MHz, CD_3OD): δ 162.27, 160.73, 155.27, 148.04, 144.89, 143.97, 142.42, 134.74, 131.98, 131.00, 130.18, 127.78, 125.83, 125.58, 123.42, 114.32, 60.10, 54.66. ESI-MS m/z : 347.0 $[M - Br]^+$; HR-ESIMS m/z : 347.1401 calcd for $C_{21}H_{19}N_2O_3^+$ (347.1396).

4.6.23. (*E*)-1-Benzyl-4-(4-ethoxystyryl)pyridin-1-ium bromide (**7w**). Yield: 95%; yellow solid; mp 251–253 °C; IR (ν_{max}): 3416, 3031, 2979, 2924, 2851, 2354, 1619, 1595, 1572, 1517, 1455, 1393, 1330, 1307, 1289, 1258, 1176, 1157, 1042, 985 cm^{-1} ; 1H NMR (400 MHz, CD_3OD): δ 8.68 (d, $J = 6.2$ Hz, 2H), 8.01 (d, $J = 6.7$ Hz, 2H), 7.80 (d, $J = 16.2$ Hz, 1H), 7.60 (d, $J = 8.8$ Hz, 2H), 7.37 (d, $J = 3.6$ Hz, 4H), 6.90 (d, $J = 8.8$ Hz, 2H), 6.78 (d, $J = 8.7$ Hz, 1H), 6.53 (d, $J = 12.1$ Hz, 1H), 5.60 (s, 2H), 4.01 (q, $J = 14.0$, 7.0 Hz, 2H), 1.32 (t, $J = 5.6$ Hz, 3H); ^{13}C NMR (126 MHz, CD_3OD): δ 161.58, 154.98, 143.54, 142.18, 133.74, 130.06, 129.45, 129.28, 128.52, 127.61, 123.49, 119.69, 114.74, 63.44, 62.93, 13.65. ESI-MS m/z : 316.0 $[M - Br]^+$; HR-ESIMS m/z : 316.1705 calcd for $C_{22}H_{22}NO^+$ (316.1701).

4.6.24. (*E*)-4-(4-Ethoxystyryl)-1-(2-methylbenzyl)pyridin-1-ium bromide (**7x**). Yield: 94%; yellow solid; mp 232–234 °C; IR (ν_{max}): 3030, 2978, 2928, 1643, 1616, 1570, 1556, 1471, 1391, 1332, 1311, 1286, 1216 982 cm^{-1} ; 1H NMR (400 MHz, CD_3OD): δ 8.56 (d, $J = 6.7$ Hz, 2H), 8.02 (d, $J = 6.7$ Hz, 2H), 7.81 (d, $J = 16.2$ Hz, 1H), 7.60 (d, $J = 8.6$ Hz, 2H), 7.31–7.20 (m, 5H), 6.90 (d, $J = 8.7$ Hz, 2H), 5.68 (s, 2H), 4.01 (q, $J = 7.0$ Hz, 2H), 2.23 (s, 3H), 1.31 (t, $J = 7.0$ Hz, 3H); ^{13}C NMR (126 MHz, CD_3OD): δ 161.57, 155.81, 143.73, 143.54, 141.44, 141.28, 131.14, 130.35, 130.23, 130.10, 129.95, 129.40, 129.37, 129.02, 127.17, 127.08, 126.84, 123.58, 123.44, 122.55, 119.70, 114.79, 114.66, 63.34, 62.53, 17.83, 13.65; ESI-MS m/z : 330.0 $[M - Br]^+$; HR-ESIMS m/z : 330.1855 calcd for $C_{23}H_{24}NO^+$ (330.1858).

4.6.25. (*E*)-4-(4-Ethoxystyryl)-1-(2-chlorobenzyl)pyridin-1-ium chloride (**7y**). Yield: 93%; yellow solid; mp 219–221 °C; IR (ν_{max}): 3036, 2980, 2932, 1620, 1572, 1469, 1393, 1331, 1309, 1291, 1204, 1175, 989 cm^{-1} ; 1H NMR (400 MHz, CD_3OD): δ 8.63 (d, $J = 6.9$ Hz, 2H), 8.02 (d, $J = 6.9$ Hz, 2H), 7.82 (d, $J = 16.2$ Hz, 1H), 7.60 (d, $J = 8.8$ Hz, 2H), 7.50–4.40 (m, 5H), 6.90 (d, $J = 8.7$ Hz, 2H), 5.75 (s, 2H), 4.01 (q, $J = 7.0$ Hz, 2H), 1.31 (t, $J = 7.0$ Hz, 3H); ^{13}C NMR (126 MHz, CD_3OD): δ 161.63, 155.22, 144.01, 143.76, 142.44, 134.31, 132.11, 131.93, 131.57, 130.91, 130.35, 130.24, 130.13, 127.99, 127.61, 126.99, 123.34, 122.58, 119.69, 114.77, 114.63, 63.47, 60.67, 13.65. ESI-MS m/z : 350.0 $[M - Cl]^+$; HR-ESIMS m/z : 350.1315 calcd for $C_{22}H_{21}ClNO^+$ (350.1312).

4.6.26. (*E*)-4-(4-Ethoxystyryl)-1-(4-chlorobenzyl)pyridin-1-ium chloride (**7z**). Yield: 95%; yellow solid; mp 208–210 °C; IR (ν_{max}): 3034, 2981, 2931, 1642, 1596, 1572, 1558, 1517, 1472, 1426, 1413, 1329, 1207, 977 cm^{-1} ; 1H NMR (400 MHz, CD_3OD): δ 8.77 (d, $J = 6.9$ Hz, 2H), 8.12 (d, $J = 6.9$ Hz, 2H), 7.91 (d, $J = 16.2$ Hz, 1H), 7.70 (m, 3H), 7.49 (br s, 4H), 7.00 (d, $J = 8.8$ Hz, 2H), 5.69 (s, 2H), 4.11 (q, $J = 7.0$ Hz, 2H), 1.41 (t, $J = 7.0$ Hz, 3H); ^{13}C NMR (126 MHz, CD_3OD): δ 161.61,

155.12, 143.78, 143.57, 142.32, 141.40, 135.46, 132.48, 130.39, 130.33, 130.24, 130.09, 129.35, 127.61, 127.15, 123.56, 122.54, 119.69, 114.77, 114.64, 63.46, 62.04, 13.65. ESI-MS m/z : 350.0 $[M - Cl]^+$; HR-ESIMS m/z : 350.1313 calcd for $C_{22}H_{21}ClNO^+$ (350.1312).

4.6.27. (*E*)-4-(4-Ethoxystyryl)-1-(2-fluorobenzyl)pyridin-1-ium bromide (**7aa**). Yield: 90%; yellow solid; mp 232–234 °C; IR (ν_{max}): 3386, 3028, 2919, 2849, 2353, 1643, 1570, 1470, 1455, 1333, 1306, 1216, 1117, 985 cm^{-1} ; 1H NMR (400 MHz, CD_3OD): δ 8.67 (d, $J = 6.7$ Hz, 2H), 8.01 (d, $J = 6.9$ Hz, 2H), 7.81 (d, $J = 16.2$ Hz, 1H), 7.76 (d, $J = 6.7$ Hz, 1H), 7.60 (d, $J = 8.8$ Hz, 2H), 7.52–7.42 (m, 2H), 6.90 (d, $J = 8.8$ Hz, 2H), 6.78 (d, $J = 8.7$ Hz, 1H), 6.53 (d, $J = 12.0$ Hz, 1H), 5.68 (s, 2H), 4.01 (q, $J = 7.0$ Hz, 2H), 1.32 (t, $J = 5.5$ Hz, 3H); ^{13}C NMR (126 MHz, CD_3OD): δ 162.24 ($^1J_{CF} = 252$ Hz), 161.65, 155.21, 143.63 ($^3J_{CF} = 30$ Hz), 132.20, 131.26, 130.34, 130.10, 127.09, 125.18, 123.46, 122.52, 119.66, 115.95 ($^2J_{CF} = 21.4$ Hz), 114.76, 63.46, 57.82 ($^3J_{CF} = 55$ Hz), 13.63. ESI-MS m/z : 334.0 $[M - Br]^+$; HR-ESIMS m/z : 334.1613 calcd for $C_{22}H_{21}FNO^+$ (334.1607).

4.6.28. (*E*)-4-(4-Ethoxystyryl)-1-(2-nitrobenzyl)pyridin-1-ium bromide (**7ab**). Yield: 87%; yellow solid; mp 209–211 °C; IR (ν_{max}): 3416, 2921, 2852, 2328, 1729, 1695, 1641, 1616, 1595, 1516, 1468, 1308, 1257, 1171, 1042 cm^{-1} ; 1H NMR (400 MHz, CD_3OD): δ 8.62 (d, $J = 6.7$ Hz, 2H), 8.21 (d, $J = 8.1$ Hz, 1H), 8.04 (d, $J = 6.7$ Hz, 2H), 7.84–7.68 (m, 4H), 7.62 (d, $J = 8.7$ Hz, 2H), 7.40 (d, $J = 7.6$ Hz, 1H), 6.91 (d, $J = 8.6$ Hz, 2H), 5.98 (s, 2H), 4.02 (q, $J = 6.9$ Hz, 2H), 1.32 (t, $J = 7.0$ Hz, 3H); ^{13}C NMR (126 MHz, $DMSO-d_6$): δ 161.20, 154.68, 147.98, 145.22, 142.19, 135.42, 130.82, 130.73, 130.53, 130.17, 128.11, 126.07, 124.09, 121.14, 115.58, 63.92, 59.88, 15.03. ESI-MS m/z : 361.0 $[M - Br]^+$; HR-ESIMS m/z : 361.1556 calcd for $C_{22}H_{21}N_2O_3^+$ (361.1552).

4.6.29. (*E*)-1-Benzyl-4-(4-bromostyryl)pyridin-1-ium bromide (**7ac**). Yield: 88%; light yellow sticky solid; IR (ν_{max}): 3416, 3033, 2922, 2851, 2345, 1652, 1641, 1620, 1583, 1558, 1514, 1467, 1455, 1404, 1336, 1241, 1156 cm^{-1} ; 1H NMR (400 MHz, CD_3OD): δ 8.79 (d, $J = 6.8$ Hz, 2H), 8.10 (d, $J = 6.8$ Hz, 2H), 7.80 (d, $J = 16.3$ Hz, 1H), 7.57–7.51 (m, 5H), 7.43–7.33 (m, 5H), 5.66 (s, 2H); ^{13}C NMR (126 MHz, CD_3OD): δ 154.21, 143.96, 140.51, 134.23, 133.57, 132.00, 130.41, 129.66, 129.53, 129.31, 128.75, 128.64, 127.43, 125.21, 124.46, 124.30, 123.23, 63.26. ESI-MS m/z : 350.0 $[M - Br]^+$; HR-ESIMS m/z : 350.0550 calcd for $C_{20}H_{17}BrN^+$ (350.0544).

4.6.30. (*E*)-4-(4-Bromostyryl)-1-(2-chlorobenzyl)pyridin-1-ium chloride (**7ad**). Yield: 86%; yellowish sticky solid; IR (ν_{max}): 3422, 3037, 2941, 2863, 2322, 1625, 1633, 1571, 1566, 1456, 1331, 1210, 1156, 1071 cm^{-1} ; 1H NMR (400 MHz, CD_3OD): δ 8.72 (d, $J = 6.7$ Hz, 2H), 8.10 (d, $J = 6.8$ Hz, 2H), 7.82 (d, $J = 16.3$ Hz, 1H), 7.60–7.33 (m, 9H), 5.79 (s, 2H); ^{13}C NMR (126 MHz, CD_3OD): δ 154.46, 144.20, 140.76, 134.38, 134.22, 132.07, 132.02, 131.67, 130.76, 130.27, 129.70, 128.02, 124.53, 124.15, 123.21, 61.00. ESI-MS m/z : 385.0 $[M - Cl]^+$; HR-ESIMS m/z : 386.0308 calcd for $C_{20}H_{16}BrClN^+$ (386.0311).

4.6.31. (*E*)-4-(4-Bromostyryl)-1-(2-fluorobenzyl)pyridin-1-ium bromide (**7ae**). Yield: 87%; yellow solid; mp 255–257 °C; IR (ν_{max}): 3424, 3032, 2930, 2853, 2322, 1667, 1522, 1482, 1407, 1331, 1250, 1212, 1157, 1065, 1022 cm^{-1} ; 1H NMR (400 MHz, CD_3OD): δ 8.77 (d, $J = 6.6$ Hz, 2H), 8.70 (d, $J = 6.6$ Hz, 2H), 8.10 (d, $J = 6.7$ Hz, 2H), 7.81 (d, $J = 16.3$ Hz, 1H), 7.73 (d, $J = 6.5$ Hz, 2H), 7.55 (d, $J = 8.2$ Hz, 2H), 7.41 (d, $J = 8.4$ Hz, 1H), 7.36 (d, $J = 16.4$ Hz, 1H), 6.73 (d, $J =$

12.1 Hz, 1H), 5.71 (s, 2H); ^{13}C NMR (126 MHz, CD_3OD): δ 162.26 ($^1J_{CF} = 249$ Hz), 154.97, 154.43, 144.19 ($^3J_{CF} = 13.9$ Hz), 140.73, 139.70, 134.22, 132.35, 132.01, 130.42, 129.70, 127.44, 125.20, 124.29, 123.21, 115.95 ($^2J_{CF} = 21.4$ Hz), 58.02 ($^3J_{CF} = 41.6$ Hz). ESI-MS m/z : 368.0 $[M - Br]^+$; HR-ESIMS m/z : 368.0450 calcd for $C_{20}H_{16}BrFN^+$ (368.0450).

4.6.32. (*E*)-4-(4-Bromostyryl)-1-(4-fluorobenzyl)pyridin-1-ium chloride (**7af**). Yield: 89%; white solid; mp 258–260 °C; IR (ν_{max}): 3425, 3026, 2933, 2846, 2331, 1625, 1593, 1522, 1461, 1332, 1215, 1166, 1063 cm^{-1} ; 1H NMR (400 MHz, CD_3OD): δ 8.77 (d, $J = 6.6$ Hz, 2H), 8.10 (d, $J = 6.7$ Hz, 2H), 7.81 (d, $J = 16.3$ Hz, 1H), 7.55–7.45 (m, 8H), 7.36 (d, $J = 16.3$ Hz, 1H), 5.63 (s, 2H); ^{13}C NMR (126 MHz, CD_3OD): δ 164.51 ($^1J_{CF} = 249.5$ Hz), 154.30, 143.90, 140.59, 134.22, 132.02, 131.12, 131.05, 129.63, 124.50, 124.32, 123.21, 116.20 ($^2J_{CF} = 22.7$ Hz), 62.40. ESI-MS m/z : 368.0 $[M - Cl]^+$; HR-ESIMS m/z : 368.0457 calcd for $C_{20}H_{16}BrFN^+$ (368.0450).

4.6.33. (*E*)-1-Benzyl-4-(4-chlorostyryl)pyridin-1-ium chloride (**7ag**). Yield: 88%; yellow solid; IR (ν_{max}): 3420, 2924, 2354, 1642, 1621, 1517, 1455, 1343, 1218, 1157, 1088, 1012 cm^{-1} ; 1H NMR (400 MHz, CD_3OD): δ 8.78 (d, $J = 6.8$ Hz, 2H), 8.10 (d, $J = 6.8$ Hz, 2H), 7.82 (d, $J = 16.3$ Hz, 1H), 7.64 (m, 3H), 7.43–7.36 (m, 7H), 5.66 (s, 2H); ^{13}C NMR (126 MHz, CD_3OD): δ 154.28, 140.47, 136.21, 133.84, 133.56, 129.53, 129.46, 129.31, 128.99, 128.58, 124.25, 123.13, 63.25. ESI-MS m/z : 306.0 $[M - Cl]^+$; HR-ESIMS m/z : 306.1054 calcd for $C_{20}H_{17}ClN^+$ (306.1050).

4.6.34. (*E*)-4-(4-Chlorostyryl)-1-(2-methylbenzyl)pyridin-1-ium bromide (**7ah**). Yield: 86%; white solid; mp 253–255 °C; IR (ν_{max}): 3415, 2924, 2853, 2351, 1621, 1589, 1516, 1491, 1409, 1214, 1151, 1086 cm^{-1} ; 1H NMR (400 MHz, CD_3OD): δ 8.65 (d, $J = 6.8$ Hz, 2H), 8.10 (d, $J = 6.8$ Hz, 2H), 7.83 (d, $J = 16.3$ Hz, 1H), 7.65 (m, 3H), 7.39–7.21 (m, 6H), 5.72 (s, 2H), 2.24 (s, 3H); ^{13}C NMR (126 MHz, CD_3OD): δ 154.28, 143.92, 140.50, 137.45, 136.19, 133.87, 131.12, 129.88, 129.49, 128.98, 127.40, 124.22, 123.17, 61.35, 17.85. ESI-MS m/z : 320.0 $[M - Br]^+$; HR-ESIMS m/z : 320.1206 calcd for $C_{21}H_{19}ClN^+$ (320.1206).

4.6.35. (*E*)-4-(4-Chlorostyryl)-1-(2-chlorobenzyl)pyridin-1-ium chloride (**7ai**). Yield: 87%; white solid; mp 146–148 °C; IR (ν_{max}): 3383, 2922, 2852, 2343, 1620, 1588, 1491, 1468, 1222, 1155, 1088, 1021 cm^{-1} ; 1H NMR (400 MHz, CD_3OD): δ 8.77 (d, $J = 6.7$ Hz, 2H), 8.10 (d, $J = 6.8$ Hz, 2H), 7.83 (d, $J = 16.3$ Hz, 1H), 7.64 (d, $J = 8.5$ Hz, 2H), 7.49–7.45 (m, 2H), 7.36–7.12 (m, 5H), 5.63 (s, 2H); ^{13}C NMR (126 MHz, CD_3OD): δ 154.30, 143.89, 140.50, 136.19, 133.85, 131.13, 131.06, 129.67, 129.48, 128.98, 124.30, 123.14, 116.19, 116.02, 62.38. ESI-MS m/z : 340.0 $[M - Cl]^+$; HR-ESIMS m/z : 340.0663 calcd for $C_{20}H_{16}Cl_2N^+$ (340.0660).

4.6.36. (*E*)-4-(4-Chlorostyryl)-1-(4-chlorobenzyl)pyridin-1-ium chloride (**7aj**). Yield: 93%; white solid; mp 123–125 °C; IR (ν_{max}): 3391, 3120, 3088, 3041, 2095, 1621, 1589, 1567, 1515, 1492, 1470, 1410, 1330, 1207, 1157, 1012, 980 cm^{-1} ; 1H NMR (400 MHz, CD_3OD): δ 8.78 (d, $J = 6.0$ Hz, 2H), 8.11 (d, $J = 6.7$ Hz, 2H), 7.83 (d, $J = 16.3$ Hz, 1H), 7.64 (d, $J = 8.5$ Hz, 2H), 7.43–7.33 (m, 7H), 5.65 (s, 2H); ^{13}C NMR (126 MHz, CD_3OD): δ 154.37, 143.99, 140.57, 136.21, 135.54, 133.84, 132.32, 130.34, 129.50, 129.37, 128.99, 124.33, 123.14, 62.34. ESI-MS m/z : 340.0 $[M - Cl]^+$; HR-ESIMS m/z : 340.0661 calcd for $C_{20}H_{16}Cl_2N^+$ (340.0660).

4.6.37. (*E*)-4-(4-Chlorostyryl)-1-(4-fluorobenzyl)pyridin-1-ium chloride (**7ak**). Yield: 88%; white solid; mp 237–239 °C; IR (ν_{max}): 2921, 2351, 1692, 1659, 1621, 1555, 1469,

1453, 1157 cm^{-1} ; ^1H NMR (400 MHz, CD_3OD): δ 8.72 (d, $J = 6.8$ Hz, 2H), 8.10 (d, $J = 6.8$ Hz, 2H), 7.84 (d, $J = 16.3$ Hz, 1H), 7.65 (d, $J = 8.5$ Hz, 2H), 7.52–7.33 (m, 7H), 5.79 (s, 2H); ^{13}C NMR (126 MHz, CD_3OD): δ 154.50, 144.18, 140.70, 136.24, 134.37, 133.84, 132.03, 131.66, 130.76, 130.26, 129.52, 128.99, 128.01, 124.12, 123.13, 60.98. ESI-MS m/z : 324.0 [M – Cl] $^+$; HR-ESIMS m/z : 324.0959 calcd for $\text{C}_{20}\text{H}_{16}\text{ClFN}^+$ (324.0955).

4.6.38. (*E*)-4-(4-Chlorostyryl)-1-(4-nitrobenzyl)pyridin-1-ium bromide (**7al**). Yield: 87%; white solid; mp 233–235 $^\circ\text{C}$; IR (ν_{max}): 2921, 2341, 1642, 1653, 1623, 1529, 1351, 1165, 1085 cm^{-1} ; ^1H NMR (400 MHz, CD_3OD): δ 8.72 (d, $J = 6.7$ Hz, 2H), 8.22 (d, $J = 8.1$ Hz, 1H), 8.13 (d, $J = 6.7$ Hz, 2H), 7.86 (d, $J = 16.3$ Hz, 2H), 7.78 (t, $J = 7.5$ Hz, 1H), 7.70 (d, $J = 7.8$ Hz, 1H), 7.66 (d, $J = 8.4$ Hz, 2H), 7.44 (d, $J = 7.6$ Hz, 1H), 7.38 (dd, $J = 12.4, 3.8$ Hz, 2H), 6.02 (s, 2H); ^{13}C NMR (126 MHz, CD_3OD): δ 158.54, 152.04, 148.35, 144.71, 143.62, 140.20, 138.68, 137.79, 136.11, 135.06, 134.19, 133.49, 132.94, 131.71, 131.22, 129.81, 129.14, 128.06, 127.11, 64.34. ESI-MS m/z : 351.0 [M – Br] $^+$; HR-ESIMS m/z : 351.0908 calcd for $\text{C}_{20}\text{H}_{16}\text{ClN}_2\text{O}_2^+$ (351.0900).

4.6.39. (*E*)-1-Benzyl-4-(3-chlorostyryl)pyridin-1-ium bromide (**7am**). Yield: 89%; white solid; mp 283–285 $^\circ\text{C}$; IR (ν_{max}): 2921, 2851, 2399, 1694, 1679, 1627, 1564, 1535, 1502, 1468, 1453, 1430, 1203, 994 cm^{-1} ; ^1H NMR (400 MHz, CD_3OD): δ 8.80 (d, $J = 6.8$ Hz, 2H), 8.11 (d, $J = 6.8$ Hz, 2H), 7.80 (d, $J = 16.3$ Hz, 1H), 7.69 (s, 1H), 7.59–7.57 (m, 1H), 7.41–7.35 (m, 8H), 5.66 (s, 2H); ^{13}C NMR (126 MHz, CD_3OD): δ 154.06, 144.02, 140.16, 137.16, 134.75, 133.56, 130.30, 130.03, 129.54, 129.31, 128.64, 127.62, 126.39, 124.46, 124.00, 63.31. ESI-MS m/z : 306.0 [M – Br] $^+$; HR-ESIMS m/z : 306.1052 calcd for $\text{C}_{20}\text{H}_{17}\text{ClN}^+$ (306.1050).

4.6.40. (*E*)-1-Benzyl-4-(4-nitrostyryl)pyridin-1-ium bromide (**7an**). Yield: 86%; white solid; mp 126–128 $^\circ\text{C}$; IR (ν_{max}): 3416, 2922, 2850, 2351, 1658, 1621, 1556, 1511, 1454, 1336, 1214, 1106 cm^{-1} ; ^1H NMR (400 MHz, CD_3OD): δ 8.86 (d, $J = 6.3$ Hz, 2H), 8.20 (t, $J = 7.6$ Hz, 4H), 7.95–7.87 (m, 4H), 7.55 (d, $J = 16.4$ Hz, 1H), 7.42–7.38 (m, 4H), 5.70 (s, 2H); ^{13}C NMR (126 MHz, CD_3OD): δ 153.53, 148.51, 144.25, 141.25, 138.88, 133.45, 129.58, 129.32, 128.84, 128.69, 126.61, 124.90, 123.79, 63.49. ESI-MS m/z : 317.0 [M – Br] $^+$; HR-ESIMS m/z : 317.1290 calcd for $\text{C}_{20}\text{H}_{17}\text{N}_2\text{O}_2^+$ (317.1290).

4.6.41. (*E/Z*)-1-(2-Methylbenzyl)-4-(4-nitrostyryl)pyridin-1-ium bromide (**7ao**). Yield: 85%; white solid; mp 260–262 $^\circ\text{C}$; IR (ν_{max}): 3256, 2918, 2355, 2327, 1653, 1641, 1622, 1558, 1512, 1453, 1340, 1102, 1005 cm^{-1} ; ^1H NMR (400 MHz, CD_3OD): δ 8.72 (d, $J = 6.8$ Hz, 2H), 8.23–8.17 (m, 4H), 7.94 (m, 4H), 7.56 (d, $J = 16.4$ Hz, 1H), 7.33–7.22 (m, 3H), 5.76 (s, 2H), 2.24 (s, 3H); ^{13}C NMR (126 MHz, $\text{DMSO}-d_6$): δ 161.91, 154.56, 148.31, 144.92, 142.11, 140.68, 131.10, 130.67, 130.42, 130.27, 127.56, 124.65, 124.27, 121.15, 115.20, 61.46, 55.94. ESI-MS m/z : 331.0 [M – Br] $^+$; HR-ESIMS m/z : 331.1449 calcd for $\text{C}_{21}\text{H}_{19}\text{N}_2\text{O}_2^+$ (331.1447).

4.6.42. (*E*)-1-(4-Fluorobenzyl)-4-(4-nitrostyryl)pyridin-1-ium chloride (**7ap**). Yield: 86%; white solid; mp 126–128 $^\circ\text{C}$; IR (ν_{max}): 2919, 2351, 1700, 1695, 1684, 1653, 1646, 1616, 1558, 1540, 1506, 1336 cm^{-1} ; ^1H NMR (400 MHz, CD_3OD): δ 8.85 (d, $J = 6.2$ Hz, 2H), 8.22 (m, 4H), 7.93–7.88 (m, 4H), 7.54–7.47 (m, 4H), 5.67 (s, 2H); ^{13}C NMR (126 MHz, CD_3OD): δ 164.54, 162.56, 153.58, 148.52, 144.20, 141.23, 138.93, 131.20, 131.13, 129.55, 128.82, 126.59, 124.91, 123.81, 116.23 ($^2J_{\text{CF}} = 21.4$ Hz), 62.63. ESI-MS m/z : 335.0 [M

– Cl] $^+$; HR-ESIMS m/z : 335.1199 calcd for $\text{C}_{20}\text{H}_{16}\text{FN}_2\text{O}_2^+$ (335.1196).

4.6.43. (*E*)-1-Benzyl-4-(2-(6-methoxynaphthalen-2-yl)-vinyl)pyridin-1-ium bromide (**7aq**). Yield: 88%; white solid; mp 281–283 $^\circ\text{C}$; IR (ν_{max}): 3407, 2922, 2852, 2345, 1642, 1608, 1556, 1516, 1481, 1454, 1391, 1264, 1219, 1157, 1022 cm^{-1} ; ^1H NMR (400 MHz, CD_3OD): δ 8.73 (d, $J = 6.9$ Hz, 2H), 8.09 (d, $J = 6.8$ Hz, 2H), 8.00–7.96 (m, 2H), 7.79–7.73 (m, 5H), 7.41–7.36 (m, 6H), 5.63 (s, 2H), 3.84 (s, 3H); ^{13}C NMR (126 MHz, CD_3OD): δ 159.45, 154.77, 143.67, 142.57, 136.26, 133.70, 130.44, 130.34, 129.96, 129.49, 129.30, 128.79, 128.52, 127.55, 127.28, 123.78, 123.65, 121.31, 119.33, 105.72, 63.05, 54.54. ESI-MS m/z : 352.0 [M – Br] $^+$; HR-ESIMS m/z : 352.1705 calcd for $\text{C}_{25}\text{H}_{22}\text{NO}^+$ (352.1701).

4.6.44. (*E*)-4-(2-(7-Methoxynaphthalen-2-yl)vinyl)-1-(2-methylbenzyl)pyridin-1-ium-bromide (**7ar**). Yield: 88%; white solid; mp 265–267 $^\circ\text{C}$; IR (ν_{max}): 2924, 2341, 1641, 1482, 1463, 1416, 1349, 1265, 1218, 1192, 1024, 973 cm^{-1} ; ^1H NMR (400 MHz, CD_3OD): δ 8.71 (d, $J = 5.4$ Hz, 2H), 8.21 (d, $J = 5.6$ Hz, 2H), 8.12–8.07 (m, 2H), 7.91–7.86 (m, 4H), 7.50–7.29 (m, 6H), 5.81 (s, 2H), 3.96 (s, 3H), 2.36 (s, 3H); ^{13}C NMR (126 MHz, CD_3OD): δ 159.35, 154.97, 143.77, 137.38, 131.12, 130.44, 130.28, 129.96, 129.90, 129.42, 128.81, 128.54, 127.55, 127.32, 127.26, 126.81, 126.01, 123.85, 123.73, 121.33, 119.30, 61.16, 54.55, 17.78. ESI-MS m/z : 366.0 [M – Br] $^+$; HR-ESIMS m/z : 366.1859 calcd for $\text{C}_{26}\text{H}_{24}\text{NO}^+$ (366.1858).

4.6.45. (*E*)-4-(2-(7-Methoxynaphthalen-2-yl)vinyl)-1-(2-chlorobenzyl)pyridin-1-ium Chloride (**7as**). Yield: 90%; brown solid; mp 256–258 $^\circ\text{C}$; IR (ν_{max}): 3356, 2930, 2859, 2343, 1703, 1650, 1632, 1539, 1526, 1469, 1341, 1223, 1171, 1025, 977 cm^{-1} ; ^1H NMR (400 MHz, CD_3OD): δ 8.68 (d, $J = 6.8$ Hz, 2H), 8.09 (d, $J = 6.8$ Hz, 2H), 8.01–7.97 (m, 2H), 7.79–7.73 (m, 4H), 7.52–7.49 (m, 2H), 7.45–7.39 (m, 2H), 7.37 (d, 2H), 5.77 (s, 2H), 3.84 (s, 3H); ^{13}C NMR (126 MHz, CD_3OD): δ 159.45, 154.98, 143.85, 142.80, 136.28, 134.34, 131.94, 130.43, 130.27, 130.01, 129.46, 128.01, 127.56, 127.17, 126.04, 123.71, 123.63, 121.30, 119.30, 105.79, 60.79, 54.58. ESI-MS m/z : 386.0 [M – Cl] $^+$; HR-ESIMS m/z : 386.1316 calcd for $\text{C}_{25}\text{H}_{21}\text{ClNO}^+$ (386.1312).

4.6.46. (*E*)-4-(2-(6-Methoxynaphthalen-2-yl)vinyl)-1-(4-chlorobenzyl)pyridin-1-ium-chloride (**7at**). Yield: 88%; brown solid; mp 153–155 $^\circ\text{C}$; IR (ν_{max}): 3389, 2919, 2850, 2353, 1670, 1642, 1609, 1555, 1516, 1454, 1350, 1263, 1192, 985 cm^{-1} ; ^1H NMR (400 MHz, CD_3OD): δ 8.72 (d, $J = 6.8$ Hz, 2H), 8.10 (d, $J = 6.8$ Hz, 2H), 8.01–7.97 (m, 2H), 7.79–7.73 (m, 5H), 7.40 (m, 5H), 5.62 (s, 2H), 3.84 (s, 3H); ^{13}C NMR (126 MHz, CD_3OD): δ 159.45, 154.88, 143.68, 142.68, 136.27, 135.51, 132.42, 130.44, 130.38, 130.31, 130.24, 129.99, 129.37, 128.78, 127.55, 127.33, 123.84, 123.68, 121.30, 119.30, 105.76, 62.15, 54.55. ESI-MS m/z : 386.0 [M – Cl] $^+$; HR-ESIMS m/z : 386.1312 calcd for $\text{C}_{25}\text{H}_{21}\text{ClNO}^+$ (386.1312).

4.6.47. (*E*)-4-(2-(7-Methoxynaphthalen-2-yl)vinyl)-1-(2-fluorobenzyl)pyridin-1-ium-bromide (**7au**). Yield: 93%; yellow solid 241–243 $^\circ\text{C}$; IR (ν_{max}): 2916, 2848, 2351, 1695, 1659, 1642, 1608, 1555, 1482, 1454, 1349, 1235, 1024 cm^{-1} ; ^1H NMR (400 MHz, CD_3OD): δ 8.71 (d, $J = 6.3$ Hz, 2H), 8.09 (d, $J = 6.3$ Hz, 2H), 7.99 (br s, 1H), 7.95 (s, 1H), 7.76 (t, $J = 10.8$ Hz, 4H), 7.65–7.01 (m, 6H), 5.72 (s, 2H), 3.84 (s, 3H); ^{13}C NMR (126 MHz, CD_3OD): δ 159.44, 154.93, 143.75, 142.74, 136.27, 132.30, 132.23, 131.33, 130.42, 129.99, 128.77, 127.54, 125.20, 125.17, 123.75, 123.69, 121.28, 120.89, 120.78, 119.30, 115.95, 115.78, 105.73, 57.46, 54.55.

ESI-MS m/z : 370.0 $[M - Br]^+$; HR-ESIMS m/z : 370.1608 calcd for $C_{25}H_{21}FNO^+$ (370.1607).

4.6.48. (E)-4-(2-(7-Methoxynaphthalen-2-yl)vinyl)-1-(4-fluorobenzyl)pyridin-1-ium Chloride (7av). Yield: 95%; yellow solid; mp 261–263 °C; IR (ν_{max}): 3387, 2920, 2850, 2344, 1642, 1609, 1556, 1508, 1482, 1468, 1390, 1264, 1230, 1193, 1025, 984 cm^{-1} ; 1H NMR (400 MHz, CD_3OD): δ 8.72 (d, J = 6.8 Hz, 2H), 8.09 (d, J = 6.9 Hz, 2H), 8.00–7.96 (m, 2H), 7.79–7.73 (m, 4H), 7.49–7.35 (m, 6H), 5.61 (s, 2H), 3.84 (s, 3H); ^{13}C NMR (126 MHz, CD_3OD): δ 159.45, 154.82, 143.60, 142.62, 136.27, 131.02 ($^3J_{CF}$ = 8.8 Hz), 130.43 ($^3J_{CF}$ = 8.8 Hz), 129.96, 128.78, 127.55, 123.80, 123.64, 121.29, 119.33, 116.20 ($^2J_{CF}$ = 22.7 Hz), 105.72, 62.18, 54.54. ESI-MS m/z : 370.0 $[M - Cl]^+$; HR-ESIMS m/z : 370.1606 calcd for $C_{25}H_{21}FNO^+$ (370.1607).

4.6.49. (E)-4-(2-(7-Methoxynaphthalen-2-yl)vinyl)-1-(2-nitrobenzyl)pyridin-1-ium-bromide (7aw). Yield: 85%; yellow solid; mp 251–253 °C; IR (ν_{max}): 3363, 2951, 2362, 1644, 1605, 1585, 1463, 1357, 1263, 1239, 1186, 1158, 1135, 1023, 985 cm^{-1} ; 1H NMR (400 MHz, CD_3OD): δ 8.67 (d, J = 6.5 Hz, 2H), 8.23 (d, J = 8.1 Hz, 1H), 8.12 (d, J = 6.6 Hz, 2H), 8.03–8.00 (m, 3H), 7.80–7.76 (m, 5H), 7.71–7.67 (m, 1H), 7.43–7.39 (m, 2H), 6.00 (s, 2H), 3.85 (s, 3H); ^{13}C NMR (126 MHz, CD_3OD): δ 159.50, 155.14, 148.08, 144.09, 142.93, 136.33, 134.69, 131.87, 131.04, 130.47, 129.99, 128.79, 127.58, 125.87, 123.66, 123.61, 121.32, 119.35, 105.73, 60.20, 54.55. ESI-MS m/z : 397.0 $[M - Br]^+$; HR-ESIMS m/z : 397.1548 calcd for $C_{25}H_{21}N_2O_3^+$ (397.1552).

4.6.50. (E)-4-(2-(7-Methoxynaphthalen-2-yl)vinyl)-1-(4-nitrobenzyl)pyridin-1-ium-bromide (7ax). Yield: 94%; yellow solid; mp 278–280 °C; IR (ν_{max}): 3362, 3011, 2921, 2352, 1642, 1607, 1555, 1518, 1484, 1346, 1265, 1234, 1196, 1157, 1104, 972 cm^{-1} ; 1H NMR (400 MHz, $DMSO-d_6$): δ 8.96 (d, J = 6.8 Hz, 2H), 8.21–8.19 (m, 4H), 8.10–8.04 (m, 3H), 7.81 (t, J = 4.4 Hz, 3H), 7.66 (d, J = 8.7 Hz, 2H), 7.51 (d, J = 16.2 Hz, 1H), 7.29 (d, J = 2.3 Hz, 1H), 5.81 (s, 2H), 3.80 (s, 3H); ^{13}C NMR (101 MHz, $DMSO-d_6$): δ 159.24, 148.38, 144.83, 142.48, 130.79, 130.54, 130.26, 128.72, 128.21, 124.79, 124.66, 124.60, 122.72, 119.90, 106.92, 55.89. ESI-MS m/z : 397.0 $[M - Br]^+$; HR-ESIMS m/z : 397.1551 calcd for $C_{25}H_{21}N_2O_3^+$ (397.1552).

4.7. Synthesis of (E)-1-benzyl-N-((2-methoxynaphthalen-6-yl)methylene)piperidin-4-amine (9a). To the solution of 6-methoxy-2-naphthaldehyde (1, equiv) and 1-benzylpiperidin-4-amine (1.5, equiv) in ethanol, few drops of glacial acetic acid were added. The resulting mixture was stirred at room temperature for 6–7 h. The solvent was evaporated on a rotary evaporator to obtain the imine product, **9a**, in 80% yield. White solid; mp 143–145 °C; IR (ν_{max}): 3436, 2949, 2851, 2800, 1628, 1602, 1553, 1480, 1384, 1246, 1169, 1024 cm^{-1} ; 1H NMR (400 MHz, $CDCl_3$): δ 8.46 (s, 1H), 8.01–7.94 (m, 2H), 7.84–7.73 (m, 2H), 7.43–7.37 (m, 3H), 7.37–7.33 (m, 1H), 7.32–7.29 (m, 1H), 7.22–7.14 (m, 2H), 3.96 (s, 3H), 3.60 (s, 2H), 3.37–3.25 (m, 1H), 3.00 (d, J = 12.2 Hz, 2H), 2.28–2.15 (m, 2H), 2.04–1.90 (m, 2H), 1.81 (t, J = 15.2 Hz, 2H); ^{13}C NMR (101 MHz, $CDCl_3$): δ 159.36, 158.60, 136.04, 132.13, 130.12, 129.45, 129.19, 128.49, 128.22, 127.24, 126.99, 124.71, 119.19, 105.96, 67.73, 63.19, 55.37, 52.18, 33.56. ESI-MS m/z : 359.0 $[M + H]^+$; HR-ESIMS m/z : 359.2122 calcd for $C_{24}H_{26}N_2O + H^+$ (359.2123).

4.8. Synthesis of 1-benzyl-N-((2-methoxynaphthalen-6-yl)methyl)piperidin-4-amine (10a). To the solution of 1-benzyl-N-((2-methoxynaphthalen-6-yl)methylene)piperidin-4-

amine (**9a**) in methanol was added sodium borohydride (2 equiv), and the mixture was stirred at room temperature for 4 h. The solvent was evaporated, and the resulting crude residue was separated in dichloromethane and water. The dichloromethane layer was dried over a rotary evaporator, and the obtained residue was purified using silica gel column chromatography using the dichloromethane: methanol mobile phase to afford **10a** as a white solid in 68% yield. mp 112–114 °C; IR (ν_{max}): 3435, 3052, 2932, 2796, 1604, 1553, 1451, 1384, 1263, 1173, 1028 cm^{-1} ; 1H NMR (400 MHz, $CDCl_3$): δ 7.58 (s, 1H), 7.58–7.51 (m, 2H), 7.34–7.25 (m, 1H), 7.18 (s, 2H), 7.17 (s, 2H), 7.13–7.08 (m, 1H), 7.04–6.97 (m, 2H), 3.80 (d, J = 6.7 Hz, 2H), 3.78 (s, 3H), 3.36 (s, 2H), 2.84–2.66 (m, 2H), 2.48–2.36 (m, 1H), 1.94–1.83 (m, 2H), 1.83–1.72 (m, 2H), 1.41–1.32 (m, 2H). ^{13}C NMR (101 MHz, $CDCl_3$): δ 157.46, 138.42, 135.71, 133.70, 129.20, 128.91, 128.20, 127.17, 126.99, 126.35, 118.81, 105.67, 63.09, 55.32, 54.18, 52.37, 50.82, 32.63. ESI-MS m/z : 361.0 $[M + H]^+$; HR-ESIMS m/z : 361.2284 calcd for $C_{24}H_{28}N_2O + H^+$ (361.2280).

4.9. Synthesis of 2-(1-benzylpiperidin-4-yl)-N-((2-methoxynaphthalen-6-yl)methyl)ethanamine (10b). To the solution of 6-methoxy-2-naphthaldehyde (1, equiv) and 2-(1-benzylpiperidin-4-yl)ethanamine (1.5, equiv) in ethanol, few drops of glacial acetic acid were added. The resulting mixture was stirred at room temperature for 6 h. The solvent was evaporated on a rotary evaporator to obtain the imine, **9b**, which was directly used for the next step. The methanolic solution of imine **9b** and sodium borohydride (2 equiv) was stirred at room temperature for 4 h. The solvent was evaporated, and the resulting crude residue was separated in dichloromethane and water. The dichloromethane layer was dried over a rotary evaporator, and the obtained residue was purified using silica gel column chromatography using the dichloromethane: methanol mobile phase to afford **10b** as a white solid in 56% yield. mp 102–104 °C; IR (ν_{max}): 3437, 3051, 2919, 2344, 1602, 1566, 1452, 1384, 1265, 1152 cm^{-1} ; 1H NMR (400 MHz, $CDCl_3$): δ 7.63 (s, 1H), 7.63–7.56 (m, 2H), 7.34–7.32 (m, 1H), 7.22 (s, 2H), 7.17 (d, J = 7.2 Hz, 2H), 7.09–7.02 (m, 3H), 3.83 (s, 3H), 3.83 (d, 2H), 3.40 (s, 2H), 2.93–2.70 (m, 2H), 2.64–2.55 (m, 2H), 1.89–1.79 (m, 2H), 1.58–1.50 (m, 2H), 1.42–1.35 (m, 2H), 1.24–1.16 (m, 3H). ^{13}C NMR (101 MHz, $CDCl_3$): δ 157.46, 138.48, 135.54, 133.71, 129.30, 129.20, 128.90, 128.15, 127.18, 126.95, 126.92, 126.43, 118.81, 105.67, 63.56, 55.32, 54.16, 53.87, 46.94, 36.89, 33.84, 32.42, 29.75. ESI-MS m/z : 389.0 $[M + H]^+$; HR-ESIMS m/z : 389.2592 calcd for $C_{26}H_{32}N_2O + H^+$ (389.2593).

4.10. In Vitro AChE and BChE Inhibition Assay. The assay followed here is the same as described in our previous work.⁴⁴ Briefly, the enzyme solution (2.5 U/mL AChE/BChE; 20 μ L) and test compound solution (inhibitor; 20 μ L) were incubated at 25 °C for 20 min. DTNB (140 μ L of 0.3 mM) followed by AtChI (20 μ L of 10 mM) solution were added. The developed yellow color was measured at 412 nm. The percent inhibition of the enzyme activity was calculated using the formula $[1 - (\text{Sample}_{\text{absorbance}}/\text{Control}_{\text{absorbance}})] \times 100$, and the IC_{50} was determined graphically using GraphPad Prism software. The enzyme kinetics for cholinesterase inhibition was carried out as described earlier.⁴⁴ The enzyme was incubated with different substrate and inhibitor concentrations, and the Lineweaver–Burk double-reciprocal plot was plotted between reaction velocity and substrate concentration. The inhibition rate constant (k_i) was calculated by replotting

the slopes of the Lineweaver–Burk plot versus inhibitor concentrations.

4.11. A β 42 Self-Aggregation Inhibition Assay. The assay is the same as described in our previous publication.²⁰ Briefly, the A β 1-42 rat peptide (Sigma-Aldrich) was dissolved in 10% w/v NH₄OH at 0.5 mg/ml. The solution was incubated for 10 min at room temperature, followed by removing NH₄OH under vacuum to obtain fluffy white powder. The powder is then reconstituted in a mixture of CH₃CN/0.3 mM Na₂CO₃/250 mM NaOH (48.4:48.4:3.2) to obtain a 200 μ M solution. The test compound was incubated with peptide solution at 10 μ M. After the incubation period, 40 μ M Thioflavin T was added to the assay solution, and fluorescence intensity was recorded with 446/490 nm excitation/emission filters set for 300 s at an interval of 30 s. The % inhibition of aggregation by the test compound was calculated using the formula $100 - (IFi/IFo \times 100)$, where IFi and IFo are the respective fluorescence intensities obtained in the presence and the absence of the inhibitor, respectively.

4.12. Cell Viability Assay. The cell viability was determined by MTT assay in primary astrocytes and J774A.1 cells. Primary astrocytes and J774A.1 were seeded at a density of 4×10^3 and 10^4 cells per well of a 96-well plate, respectively. Cells were treated with various concentrations of 7av (0.78 to 100 μ M) for 24 h. After drug incubation, MTT was added at a concentration of 2.5 mg/mL for 4 h. The supernatants were discarded, and DMSO was added into the wells for dissolving formazan crystals. The absorbance was measured at 570 nm.

4.13. NLRP3 Inflammasome Assay. NLRP3 inflammasome assay was done in J774A.1 cells, which were activated by LPS (1 μ g/mL) and nigericin (10 μ M). Cells were treated with various concentrations (5, 10, 20, and 40 μ M) of 7av 1 h prior to treatment with nigericin. MCC950 at 100 nM was used as the standard and added to cells 1 h before treatment with nigericin. After the treatments, the supernatant was collected for analysis of IL-1 β through ELISA. Furthermore, the remaining cells were collected and lysed with lysis buffer (0.2 N NaOH + 1% Triton X-100) for protein estimation. The level of pro-inflammatory cytokine IL-1 β in the supernatant was assessed by using an Invitrogen mL-1 β ELISA kit, and the OD values were normalized by the total protein present in the sample.

4.14. Molecular Docking. The crystal structures of human AChE (PDB ID: 4EY7)⁴⁵ and human BChE (PDB ID: 6EP4)⁴⁶ were retrieved from a PDB and were used for molecular modeling studies under default settings from Glide. The docking was performed as described earlier.⁴⁴ Briefly, the protein was made ready for docking using the protein preparation wizard tool. The bond angle and bond orders were assigned in Prep wizard; subsequently, hydrogen atoms, missing loops, and side chains were included. The restrained minimization of protein conformation was performed with an RMSD cutoff of 0.30 Å and the OPLS-2005 force field. Ligands were drawn in ChemDraw and saved in the mol2 format. LigPrep was used for preparing these ligands ready for docking. The grid was generated on the protein using a co-crystallized ligand as a centroid. Docking was performed in the XP mode under default settings of Glide. The docked poses were analyzed, and the pose with highest dock score was used for interaction analysis.

4.15. Molecular Dynamics Simulation. The stability of docked complexes was assessed via performing MD simulation using Desmond, as described earlier.⁴⁷ The protein–ligand

docked complex (.pv file) retrieved from XP docking was imported into the Maestro terminal of Desmond. Next, the system build-up was performed using the system builder, followed by minimization of the protein–ligand complex using a minimization module. The MD simulation was run for 100 ns trajectory, and results were obtained using the simulation interaction diagram module.

■ ASSOCIATED CONTENT

SI Supporting Information

The Supporting Information is available free of charge at <https://pubs.acs.org/doi/10.1021/acsomega.2c08167>.

Scanned copies of ¹H and ¹³C NMR spectra and HRMS of all compounds and time frame analysis of 7av-AChE and 7av-BChE interaction during 100 ns MD simulation (PDF)

■ AUTHOR INFORMATION

Corresponding Author

Sandip B. Bharate – *Natural Products & Medicinal Chemistry Division, CSIR-Indian Institute of Integrative Medicine, Jammu 180001, India; Academy of Scientific & Innovative Research (AcSIR), Ghaziabad 201002, India;* orcid.org/0000-0001-6081-5787; Phone: +91-191-2586333; Email: sbharate@iiim.res.in, sandipbharate@gmail.com

Authors

Mohd Abdulla – *Natural Products & Medicinal Chemistry Division, CSIR-Indian Institute of Integrative Medicine, Jammu 180001, India; Academy of Scientific & Innovative Research (AcSIR), Ghaziabad 201002, India*

Razia Banoo – *Natural Products & Medicinal Chemistry Division, CSIR-Indian Institute of Integrative Medicine, Jammu 180001, India; Academy of Scientific & Innovative Research (AcSIR), Ghaziabad 201002, India*

Vijay K. Nuthakki – *Natural Products & Medicinal Chemistry Division, CSIR-Indian Institute of Integrative Medicine, Jammu 180001, India; Academy of Scientific & Innovative Research (AcSIR), Ghaziabad 201002, India;* orcid.org/0000-0002-7454-1948

Mohit Sharma – *Natural Products & Medicinal Chemistry Division, CSIR-Indian Institute of Integrative Medicine, Jammu 180001, India; Academy of Scientific & Innovative Research (AcSIR), Ghaziabad 201002, India*

Sukhleen Kaur – *Pharmacology Division, CSIR-Indian Institute of Integrative Medicine, Jammu 180001, India; Academy of Scientific & Innovative Research (AcSIR), Ghaziabad 201002, India*

Shikha Thakur – *Department of Pharmacy, Birla Institute of Technology and Sciences Pilani, Pilani 333031 Rajasthan, India*

Ajay Kumar – *Pharmacology Division, CSIR-Indian Institute of Integrative Medicine, Jammu 180001, India; Academy of Scientific & Innovative Research (AcSIR), Ghaziabad 201002, India*

Hemant R. Jadhav – *Department of Pharmacy, Birla Institute of Technology and Sciences Pilani, Pilani 333031 Rajasthan, India*

Complete contact information is available at: <https://pubs.acs.org/doi/10.1021/acsomega.2c08167>

Author Contributions

M.A. and R.B. contributed equally to this work and shared first authorship. The manuscript was written through the contributions of all authors. All authors have approved the final version of the paper. M.A. and R.B. performed synthesis of compounds and docking studies; M.S. helped in synthesis of few compounds; V.K.N. performed biological evaluations; S.K. performed cytotoxicity studies; A.K. designed and mentored cytotoxicity study; S.T. performed MD simulation studies, and H.R.J. monitored and interpreted MD results. S.B.B. designed and coordinated all this work. M.A. and S.B.B. wrote the manuscript. IIM publication number: CSIR-IIM/IPR/00280.

Notes

The authors declare no competing financial interest.

ACKNOWLEDGMENTS

M.A. thanks UGC for the research fellowship. The financial support from the CSIR YSA grant (P90807) is gratefully acknowledged.

ABBREVIATIONS

ACh, acetylcholine; AChE, acetylcholinesterase; ACN, acetonitrile; AD, Alzheimer's disease; BBB, blood–brain barrier; CAS, catalytic anionic site; DMSO, dimethyl sulfoxide; EeAChE, acetylcholinesterase from *Electrophorus electricus* (electric eel); eqBChE, equine serum butyrylcholinesterase; k_i , inhibition rate constant; NLRP3 inflammasome, nucleotide-binding domain, leucine-rich–containing family, pyrin domain–containing-3 inflammasome; PAS, peripheral anionic site; PDB, Protein Data Bank; rHuAChE, recombinant human acetylcholinesterase; RMSD, root mean square deviation; RMSF, root mean square fluctuation

REFERENCES

- (1) Jahn, H. Memory loss in Alzheimer's disease. *Dialogues Clin. Neurosci.* **2013**, *15*, 445–454.
- (2) 2020 Alzheimer's disease facts and figures. *Alzheimer's Dementia* **2020**, *16*, 391–460. DOI: 10.1002/alz.12068
- (3) Goedert, M.; Spillantini, M. G. A century of Alzheimer's disease. *Science* **2006**, *314*, 777–781.
- (4) Jalili-Baleh, L.; Nadri, H.; Moradi, A.; Bukhari, S. N. A.; Shakibaie, M.; Jafari, M.; Golshani, M.; Homayouni Moghadam, F.; Firoozpour, L.; Asadipour, A.; Emami, S.; Khoobi, M.; Foroumadi, A. New racemic annulated pyrazolo[1,2-b]phthalazines as tacrine-like AChE inhibitors with potential use in Alzheimer's disease. *Eur. J. Med. Chem.* **2017**, *139*, 280–289.
- (5) Chen, G.-f.; Xu, T.-h.; Yan, Y.; Zhou, Y.-r.; Jiang, Y.; Melcher, K.; Xu, H. E. Amyloid beta: structure, biology and structure-based therapeutic development. *Acta Pharmacol. Sin.* **2017**, *38*, 1205–1235.
- (6) Hampel, H.; Mesulam, M. M.; Cuello, A. C.; Farlow, M. R.; Giacobini, E.; Grossberg, G. T.; Khachaturian, A. S.; Vergallo, A.; Cavedo, E.; Snyder, P. J.; Khachaturian, Z. S. The cholinergic system in the pathophysiology and treatment of Alzheimer's disease. *J. Neurol.* **2018**, *141*, 1917–1933.
- (7) Bekris, L. M.; Yu, C.-E.; Bird, T. D.; Tsuang, D. W. Review Article: Genetics of Alzheimer Disease. *J. Geriatr. Psychiatr. Neurol.* **2010**, *23*, 213–227.
- (8) Singh, S. K.; Srivastav, S.; Yadav, A. K.; Srikrishna, S.; Perry, G. Overview of Alzheimer's Disease and Some Therapeutic Approaches Targeting A β by Using Several Synthetic and Herbal Compounds. *Oxid. Med. Cell. Longev.* **2016**, *2016*, 1–22.
- (9) Holtzman, D. M.; Morris, J. C.; Goate, A. M. Alzheimer's disease: the challenge of the second century. *Sci. Transl. Med.* **2011**, *3*, 77sr71.
- (10) Tatulian, S. A. Challenges and hopes for Alzheimer's disease. *Drug Discov. Today* **2022**, *27*, 1027–1043.
- (11) Hshieh, T. T.; Fong, T. G.; Marcantonio, E. R.; Inouye, S. K. Cholinergic deficiency hypothesis in delirium: a synthesis of current evidence. *J. Gerontol. A Biol. Sci.* **2008**, *63*, 764–772.
- (12) Chen, Z. R.; Huang, J. B.; Yang, S. L.; Hong, F. F. Role of Cholinergic Signaling in Alzheimer's Disease. *Molecules* **2022**, *27*, 1816.
- (13) H Ferreira-Vieira, T.; M Guimaraes, I.; R Silva, F.; M Ribeiro, F. Alzheimer's disease: Targeting the Cholinergic System. *Curr. Neuropharmacol.* **2016**, *14*, 101–115.
- (14) Carvajal, F. J.; Inestrosa, N. C. Interactions of AChE with A β Aggregates in Alzheimer's Brain: Therapeutic Relevance of IDN 5706. *Front. Mol. Neurosci.* **2011**, *4*, 19.
- (15) Inestrosa, N. C.; Alvarez, A.; Pérez, C. A.; Moreno, R. D.; Vicente, M.; Linker, C.; Casanueva, O. I.; Soto, C.; Garrido, J. Acetylcholinesterase Accelerates Assembly of Amyloid- β -Peptides into Alzheimer's Fibrils: Possible Role of the Peripheral Site of the Enzyme. *Neuron* **1996**, *16*, 881–891.
- (16) Dinamarca, M. C.; Sagal, J. P.; Quintanilla, R. A.; Godoy, J. A.; Arrázola, M. S.; Inestrosa, N. C. Amyloid- β -Acetylcholinesterase complexes potentiate neurodegenerative changes induced by the A β peptide. Implications for the pathogenesis of Alzheimer's disease. *Mol. Neurodegener.* **2010**, *5*, 4.
- (17) Colović, M. B.; Krstić, D. Z.; Lazarević-Pašti, T. D.; Bondžić, A. M.; Vasić, V. M. Acetylcholinesterase inhibitors: pharmacology and toxicology. *Curr. Neuropharmacol.* **2013**, *11*, 315–335.
- (18) Wang, Y.; Wang, H.; Chen, H.-z. AChE Inhibition-based Multi-target-directed Ligands, a Novel Pharmacological Approach for the Symptomatic and Disease-modifying Therapy of Alzheimer's Disease. *Curr. Neuropharmacol.* **2016**, *14*, 364–375.
- (19) Nordberg, A.; Ballard, C.; Bullock, R.; Darreh-Shori, T.; Somogyi, M. A review of butyrylcholinesterase as a therapeutic target in the treatment of Alzheimer's disease. *Prim Care Companion CNS Disord* **2013**, *15*, 12r01412.
- (20) Abdullaha, M.; Nuthakki, V. K.; Bharate, S. B. Discovery of methoxy-naphthyl linked N-(1-benzylpiperidine) benzamide as a blood-brain permeable dual inhibitor of acetylcholinesterase and butyrylcholinesterase. *Eur. J. Med. Chem.* **2020**, *207*, 112761.
- (21) Giacobini, E. Cholinesterase inhibitors: new roles and therapeutic alternatives. *Pharmacol. Res.* **2004**, *50*, 433–440.
- (22) Mesulam, M.; Guillozet, A.; Shaw, P.; Quinn, B. Widely spread butyrylcholinesterase can hydrolyze acetylcholine in the normal and Alzheimer brain. *Neurobiol. Dis.* **2002**, *9*, 88–93.
- (23) Kandiah, N.; Pai, M. C.; Senanarong, V.; Looi, I.; Ampil, E.; Park, K. W.; Karanam, A. K.; Christopher, S. Rivastigmine: the advantages of dual inhibition of acetylcholinesterase and butyrylcholinesterase and its role in subcortical vascular dementia and Parkinson's disease dementia. *Clin. Interventions Aging* **2017**, *12*, 697–707.
- (24) S Schneider, L. A critical review of cholinesterase inhibitors as a treatment modality in Alzheimer's disease. *Dialogues Clin. Neurosci.* **2000**, *2*, 111–128.
- (25) Sharma, K. Cholinesterase inhibitors as Alzheimer's therapeutics (Review). *Mol. Med. Rep.* **2019**, *20*, 1479–1487.
- (26) Grossberg, G. T. Cholinesterase Inhibitors for the Treatment of Alzheimer's Disease: *Current Therapeutic Research* **2003**, *64*, 216–235.
- (27) Vignaux, P. A.; Minerali, E.; Lane, T. R.; Foil, D. H.; Madrid, P. B.; Puhl, A. C.; Ekins, S. The Antiviral Drug Tilorone Is a Potent and Selective Inhibitor of Acetylcholinesterase. *Chem. Res. Toxicol.* **2021**, *34*, 1296–1307.
- (28) Oinonen, P. P.; Jokela, J. K.; Hatakka, A. I.; Vuorela, P. M. Linarin, a selective acetylcholinesterase inhibitor from *Mentha arvensis*. *Fitoterapia* **2006**, *77*, 429–434.
- (29) Zanon, V. S.; Lima, J. A.; Amaral, R. F.; Lima, F. R. S.; Kitagawa, D. A. S.; Franca, T. C. C.; Vargas, M. D. Design, synthesis, molecular modeling and neuroprotective effects of a new framework of cholinesterase inhibitors for Alzheimer's disease. *J. Biomol. Struct. Dyn.* **2021**, *39*, 6112–6125.

- (30) de Souza, G. A.; da Silva, S. J.; Del Cistia, C. d. N.; Pitasse-Santos, P.; Pires, L. d. O.; Passos, Y. M.; Cordeiro, Y.; Cardoso, C. M.; Castro, R. N.; Sant'Anna, C. M. R.; Kummerle, A. E. Discovery of novel dual-active 3-(4-(dimethylamino)phenyl)-7-aminoalkoxy-coumarin as potent and selective acetylcholinesterase inhibitor and antioxidant. *J. Enzyme Inhib. Med. Chem.* **2019**, *34*, 631–637.
- (31) McHardy, S. F.; Wang, H. Y. L.; McCowen, S. V.; Valdez, M. C. Recent advances in acetylcholinesterase Inhibitors and Reactivators: an update on the patent literature (2012-2015). *Expert Opin. Ther. Pat.* **2017**, *27*, 455–476.
- (32) Meena, V. K.; Chaturvedi, S.; Sharma, R. K.; Mishra, A. K.; Hazari, P. P. Potent Acetylcholinesterase Selective and Reversible Homodimeric Agent Based on Tacrine for Theranostics. *Mol. Pharm.* **2019**, *16*, 2296–2308.
- (33) Wang, Z. F.; Yan, J.; Fu, Y.; Tang, X. C.; Feng, S.; He, X. C.; Bai, D. L. Pharmacodynamic study of FS-0311: a novel highly potent, selective acetylcholinesterase inhibitor. *Cell. Mol. Neurobiol.* **2008**, *28*, 245–261.
- (34) Stavrakov, G.; Philipova, I.; Lukarski, A.; Atanasova, M.; Georgiev, B.; Atanasova, T.; Konstantinov, S.; Doytchinova, I. Discovery of a Novel Acetylcholinesterase Inhibitor by Fragment-Based Design and Virtual Screening. *Molecules* **2021**, *26*, 2058.
- (35) Omura, S.; Kuno, F.; Otoguro, K.; Sunazuka, T.; Shiomi, K.; Masuma, R.; Iwai, Y. Arisugacin, a novel and selective inhibitor of acetylcholinesterase from *Penicillium* sp. FO-4259. *J. Antibiot.* **1995**, *48*, 745–746.
- (36) Otoguro, K.; Kuno, F.; Omura, S. Arisugacins, selective acetylcholinesterase inhibitors of microbial origin. *Pharmacol. Ther.* **1997**, *76*, 45–54.
- (37) Shrivastava, S. K.; Srivastava, P.; Upendra, T. V. R.; Tripathi, P. N.; Sinha, S. K. Design, synthesis and evaluation of some N-methylenebenzenamine derivatives as selective acetylcholinesterase (AChE) inhibitor and antioxidant to enhance learning and memory. *Bioorg. Med. Chem.* **2017**, *25*, 1471–1480.
- (38) Boulebd, H.; Ismaili, L.; Bartolini, M.; Bouraiou, A.; Andrisano, V.; Martin, H.; Bonet, A.; Moraleda, I.; Iriepa, I.; Chioua, M.; Belfaitah, A.; Marco-Contelles, J. Imidazopyranotacrines as Non-Hepatotoxic, Selective Acetylcholinesterase Inhibitors, and Antioxidant Agents for Alzheimer's Disease Therapy. *Molecules* **2016**, *21*, 400.
- (39) Jiang, C. S.; Ge, Y. X.; Cheng, Z. Q.; Song, J. L.; Wang, Y. Y.; Zhu, K.; Zhang, H. Discovery of new multifunctional selective acetylcholinesterase inhibitors: structure-based virtual screening and biological evaluation. *J. Comput. Aided Mol. Des.* **2019**, *33*, 521–530.
- (40) Mohamed, T.; Osman, W.; Tin, G.; Rao, P. P. Selective inhibition of human acetylcholinesterase by xanthine derivatives: in vitro inhibition and molecular modeling investigations. *Bioorg. Med. Chem. Lett.* **2013**, *23*, 4336–4341.
- (41) Augustin, N.; Nuthakki, V. K.; Abdullaha, M.; Hassan, Q. P.; Gandhi, S. G.; Bharate, S. B. Discovery of Helminthosporin, an Anthraquinone Isolated from *Rumex abyssinicus* Jacq as a Dual Cholinesterase Inhibitor. *ACS Omega* **2020**, *5*, 1616–1624.
- (42) Eyer, P. The role of oximes in the management of organophosphorus pesticide poisoning. *Toxicol. Rev.* **2003**, *22*, 165–190.
- (43) Abdullaha, M.; Mohammed, S.; Ali, M.; Kumar, A.; Vishwakarma, R. A.; Bharate, S. B. Discovery of Quinazolin-4(3 H)-ones as NLRP3 Inflammasome Inhibitors: Computational Design, Metal-Free Synthesis, and in Vitro Biological Evaluation. *J. Org. Chem.* **2019**, *84*, 5129–5140.
- (44) Nuthakki, V. K.; Sharma, A.; Kumar, A.; Bharate, S. B. Identification of embelin, a 3-undecyl-1,4-benzoquinone from *Embelia ribes* as a multitargeted anti-Alzheimer agent. *Drug Dev. Res.* **2019**, *80*, 655–665.
- (45) Cheung, J.; Rudolph, M. J.; Burshteyn, F.; Cassidy, M. S.; Gary, E. N.; Love, J.; Franklin, M. C.; Height, J. J. Structures of human acetylcholinesterase in complex with pharmacologically important ligands. *J. Med. Chem.* **2012**, *55*, 10282–10286.
- (46) Rosenberry, T. L.; Brazzolotto, X.; Macdonald, I. R.; Wandhammer, M.; Trovaslet-Leroy, M.; Darvesh, S.; Nachon, F. Comparison of the binding of reversible inhibitors to human butyrylcholinesterase and acetylcholinesterase: A crystallographic, kinetic and calorimetric study. *Molecules* **2017**, *22*, No. E2098.
- (47) Joshi, P.; McCann, G. J. P.; Sonawane, V. R.; Vishwakarma, R. A.; Chaudhuri, B.; Bharate, S. B. Identification of Potent and Selective CYP1A1 Inhibitors via Combined Ligand and Structure-Based Virtual Screening and Their in Vitro Validation in Saccharosomes and Live Human Cells. *J. Chem. Inf. Model.* **2017**, *57*, 1309–1320.